Meteorological factors control debris slides and debris flows in a high-Arctic glacier basin (Ny-Ålesund, Svalbard)

Erik Kuschel, Florian Tolle, Vinzent Klaus, Ursula Laa, Alexander Prokop, Jean-Michel Friedt, Eric Bernard, Christian Zangerl

▶ **To cite this version:**

Erik Kuschel, Florian Tolle, Vinzent Klaus, Ursula Laa, Alexander Prokop, et al.. Meteorological factors control debris slides and debris flows in a high-Arctic glacier basin (Ny-Ålesund, Svalbard). Geomorphology, 2024, 467, pp.109492. 10.1016/j.geomorph.2024.109492 . hal-04765289

HAL Id: hal-04765289
https://hal.science/hal-04765289v1

Submitted on 3 Dec 2024

HAL is a multi-disciplinary open access archive for the deposit and dissemination of scientific research documents, whether they are published or not. The documents may come from teaching and research institutions in France or abroad, or from public or private research centers.

L'archive ouverte pluridisciplinaire **HAL**, est destinée au dépôt et à la diffusion de documents scientifiques de niveau recherche, publiés ou non, émanant des établissements d'enseignement et de recherche français ou étrangers, des laboratoires publics ou privés.

Distributed under a Creative Commons Attribution 4.0 International License

Geomorphology 467 (2024) 109492

Contents lists available at ScienceDirect

Geomorphology

journal homepage: www.journals.elsevier.com/geomorphology

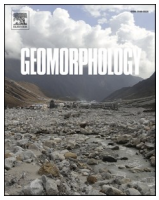

Meteorological factors control debris slides and debris flows in a high-Arctic glacier basin (Ny-Ålesund, Svalbard)

Erik Kuschel [a,*], Florian Tolle [b], Vinzent Klaus [c], Ursula Laa [d], Alexander Prokop [e,f], Jean-Michel Friedt [g], Eric Bernard [b], Christian Zangerl [a]

[a] Institute of Applied Geology, University of Natural Resources and Life Sciences, Vienna, Austria
[b] Université de Franche-Comté, CNRS, ThéMA, Besançon, France
[c] Institute of Meteorology and Climatology, University of Natural Resources and Life Sciences, Vienna, Austria
[d] Institute of Statistics, University of Natural Resources and Life Sciences, Vienna, Austria
[e] Snow Scan GmbH, Vienna, Austria
[f] University of Vienna, Department of Geodynamics and Sedimentology, Vienna, Austria
[g] Université de Franche-Comté, FEMTO-ST, Time & Frequency, Besançon, France

ARTICLE INFO

Keywords:
Landslides
Paraglacial geomorphology
Remote sensing
Terrestrial laser scanning
Svalbard
Arctic
Climate change

ABSTRACT

Landslide processes are one of the dominant agents of erosion and sediment transport on sediment-mantled slopes in arctic environments. Increased landslide activity is anticipated as climate change is projected to decrease mountain slope stability. High-Arctic environments, such as Svalbard, serve as crucial observatories for investigating current and future slope dynamics within a changing climate, particularly due to arctic amplification effects. Despite the significance of Arctic regions, empirical evidence in high latitudes is often lacking. This scarcity can be attributed to the absence of long-term, high-resolution terrain data with sufficient temporal resolution to assess the impact of meteorological boundary conditions on landscapes altered by climate change. However, addressing this gap in empirical evidence is essential for understanding the complex interplay between meteorological variables and debris slide and debris flow evolution in Arctic environments. This study presents a unique high-resolution remote sensing dataset within a high-Arctic glacier basin acquired over a 10-year period. Through the combination of terrestrial laser-scanning and an autonomous camera network, we were able to investigate the impact of meteorological boundary conditions on the trigger mechanisms of translational debris slides and debris flows and unravel paraglacial slope evolution following recent glacier retreat on the example of the Austre Lovénbreen glacier basin (Svalbard, Norway). Translational debris slides accounted for approximately 96 % ($N = 147$) of the total sediment flux observed, with debris flows ($N = 21$) acting as a secondary agent of sediment transport. The debris slide activity significantly increased between 2011 and 2021. Heavy rainfall events primarily influence the frequency and magnitude of debris slides during the hydrological summer, while the duration and intensity of the thawing period serve as the principal control for their initiation. Furthermore, a 2-year recurrence period for major debris flows ($\geq 400\ m^3$) was found, which is about 2.5 to 5 times shorter than previous estimates for the last few decades on Svalbard. In conclusion, this study highlights the impact of meteorological factors on debris slide frequency and magnitude within high-Arctic glacier basins, shedding light on the dynamics of paraglacial slope modification in Arctic environments affected by climate change.

1. Introduction

Landslides are a mass of rock, debris or earth moving down a slope (Cruden, 1991), which develop in time through several stages (Terzaghi, 1950). Landslides are one of the most dominant erosion and sediment transport processes in mountainous terrain and often pose a significant risk to communities and infrastructure worldwide (Zangerl et al., 2008; Gariano and Guzzetti, 2016). Climate change influences a wide range of factors (e.g. glacier retreat, permafrost thaw, heavy rainfall events), which are projected to decrease the stability of mountain slopes (IPCC, 2014). From a theoretical view, there are clear indicators that climate change will lead to increased landslide activity (Crozier, 2010; Huggel

* Corresponding author.
E-mail address: erik.kuschel@boku.ac.at (E. Kuschel).

https://doi.org/10.1016/j.geomorph.2024.109492
Received 14 May 2024; Received in revised form 28 October 2024; Accepted 28 October 2024
Available online 31 October 2024
0169-555X/© 2024 The Authors. Published by Elsevier B.V. This is an open access article under the CC BY license (http://creativecommons.org/licenses/by/4.0/).

et al., 2012; Seneviratne et al., 2012; Gariano and Guzzetti, 2016). However, empirical evidence is often lacking as meteorological boundary conditions altered by climate change may have different and often contrasting effects on landslide processes (IPCC, 2014; Gariano and Guzzetti, 2016).

Svalbard is a particularly important observatory for investigating current and future landslide dynamics due to its unique combination of high-latitude conditions and varied topography. The importance of this region is further emphasized by the observed pattern of global temperature increases, which are amplified with both latitude and elevation (Pepin et al., 2015; Francis et al., 2017). Notably, the Arctic has experienced annual average temperature rises up to four times greater than the global mean in recent decades (Masson-Delmotte et al., 2006; Patton et al., 2019; IPCC, 2021). Svalbard's rapidly changing climate, coupled with its extensive environmental data records (e.g. meteorological data; orthophotos since the 1920s, Fig. 1) provides a critical reference point for assessing the broader implications of climate change on geomorphic changes in high-latitude and high-elevation regions.

The term "landslide" is used to refer to the types of material and slope movements in the classification framework developed by Cruden and Varnes (1996) and updated by Hungr et al. (2014), encompassing debris slides, debris flows and rock falls relevant to this study. This terminology offers a systematic approach for categorizing and understanding the various mechanisms and processes involved in landslide phenomena, thereby facilitating a precise evaluation of their formation, behaviour, and impact within this rapidly changing landscape. Furthermore, it avoids inconsistencies (e.g. language differences, classification systems), which have previously obscured the ability to link changes in landslide frequency and magnitude to climate change at a regional scale (Wood et al., 2020) and follows recent studies focusing on landslide responses to climate change (e.g. Gariano and Guzzetti, 2016; Patton et al., 2019).

In this study, we focus our analysis on the formation and quantification of translational debris slides and debris flows, within the Austre Lovénbreen basin. Translational debris slides are characterised by the downslope movement of debris on a planar rupture surface, which may develop flow-like features after moving a specific travel distance (Hungr et al., 2014). Debris is defined as a mixture of sand, gravel, cobbles, and boulders, often with varying proportions of silt and clay, but normally with 20 to 80 % of the particles being larger than 2 mm (Cruden and Varnes, 1996; Hungr et al., 2014). Besides this, other termini found in literature such as "thermokarst features" often includes various types of debris slides or flows (e.g. Bowden et al., 2008; Hong et al., 2014; Patton et al., 2019); "cryogenic landslide" may be used to specify landslides that occur due to ice-related processes (e.g. Leibman, 1995; Leibman et al., 2014); or active layer detachments used within permafrost literature revering to thermal parameters (e.g. Ballantyne, 2002; Lewkowicz

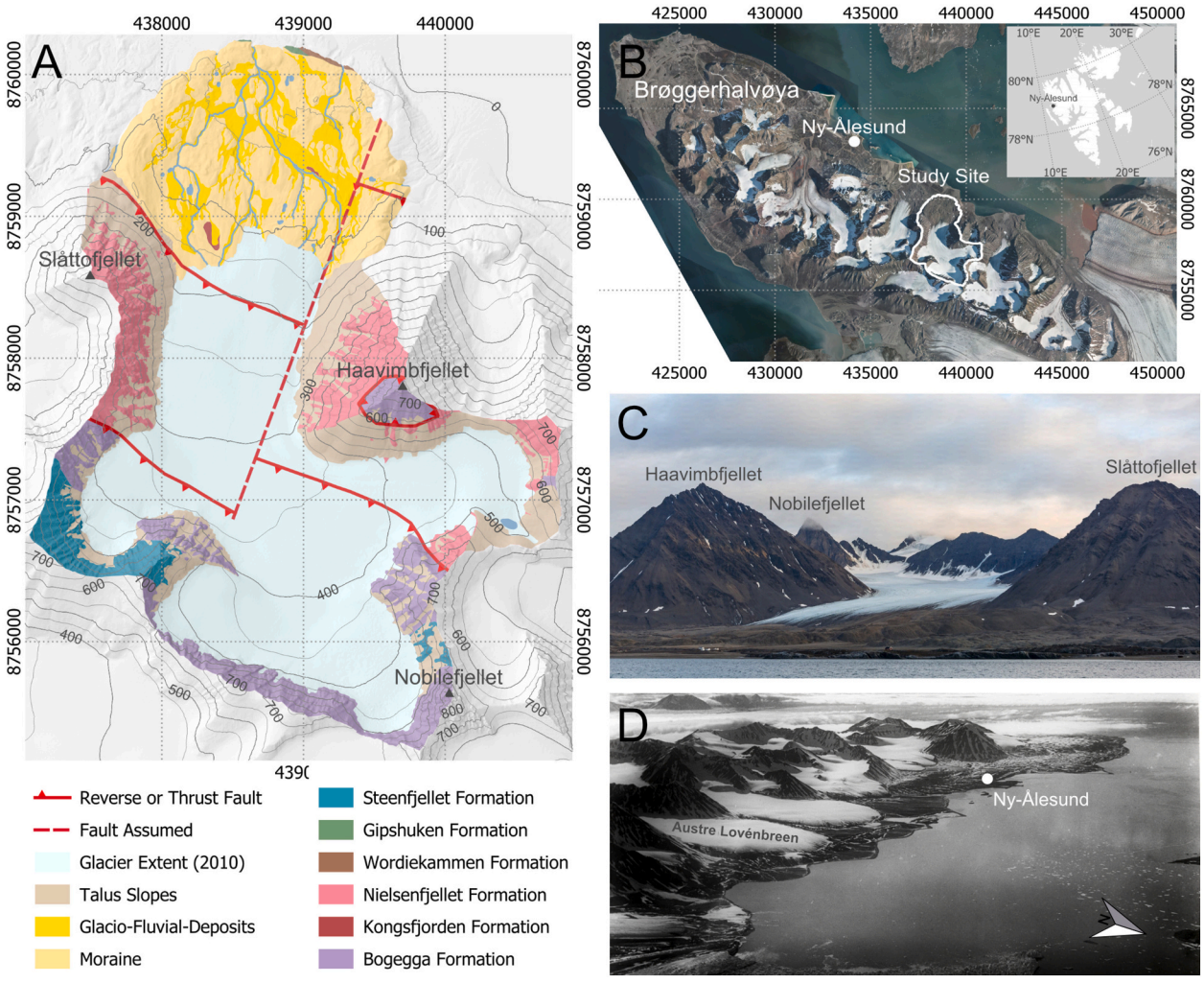

Fig. 1. Geographical and geological setting of the Austre Lovénbreen study site. A) Geological map of the study site based on the field surveys; Lineations of structural features adopted from Hjelle et al. (1999); B) overview map of the Brøggerhalvøya with Ny-Ålesund and the Study site; C) extent of the Austre Lovénbreen glacier in 2017 as seen from NW, with surrounding mountain peaks; D) historical photograph from 1923 showing the maximum post-Little Ice Age extent of the Brøggerhalvøya glaciers (Mittelholzer, 1923).

and Harris, 2005; French, 2013). Debris flows are rapid and long runout surging flows of water-saturated debris in established gullies or drainage channels, entraining material along their flow path, which may lead to the formation of debris fans and levees (Ballantyne, 2002; Hungr et al., 2014; De Haas et al., 2015).

Paraglacial slopes, as found in this region, are constantly subjected to terrain modifications through gravitational mass wasting processes (e.g. landslides, surface wash, and snow avalanches), due to the rapid adjustment of recently deglaciated landscapes to nonglacial conditions (Church and Ryder, 1972; Ballantyne, 2002). This temporal and spatial evolution of rock walls and drift-mantled slopes via various processes can be seen in the vast areas of reworked sediment draped over the slopes of Svalbard (Lønne and Lysså, 2005; De Haas et al., 2015; Lønne, 2017).

The impact of debris slides and debris flows on paraglacial slopes is well documented by many authors and embedded in the paraglacial concept (Church and Ryder, 1972; Ballantyne, 2002) and the ongoing paraglacial response of sediment-mantled slopes through these processes has been assessed and mapped (Rapp, 1960; Tolgensbakk and Sollid, 1980; Curry, 1999; Mercier et al., 2009; De Haas et al., 2015; Ewertowski and Tomczyk, 2020; Tomczyk, 2021). However, data on the impact of meteorological factors such as phases with heavy rainfall and elevated temperature on the formation of debris slides and debris flows are rare, especially for the high-Arctic environment. The reason for this is the lack of long-term terrain data, with a spatiotemporal resolution high enough to detect slope processes reaching thicknesses of only a few meters, as suggested by Patton et al. (2019).

This study attempts to fill data gaps by applying multi-temporal terrestrial laser scanning on slopes of the Austre Lovénbreen glacier basin in Svalbard to investigate the formation characteristics and the temporal evolution of debris slides and debris flows under climate change. Thus, the objectives of this study are i) to provide multi-temporal high-resolution terrestrial laser scan data, ii) to comprehensively identify, characterise, and quantify terrain changes, and iii) investigating the triggering factors for the spatiotemporal evolution of debris slides and debris flows within the Austre Lovénbreen Basin. Furthermore, we show that debris slides are the primary source of sediment transport on steep sediment-mantled slopes in a high-Arctic glacier valley and that meteorological factors significantly influence their spatial and temporal development.

2. The Austre Lovénbreen glacier basin

The Austre Lovénbreen basin is dominated by the Austre Lovénbreen glacier, a small land-based polythermal glacier (Irvine-Fynn et al., 2011) with an elevation ranging from 50 to 550 m a.s.l. The glacier has shown a constant but irregular retreat since the Little Ice Age, and in 2013, it covered a surface area of 4.61 km^2, <43 % of the total basin surface of approximately 10.45 km^2. In contrast, the glacier covered almost the entire proglacial area in the 1930s and about 50 % of the basin in the 1980s (Hagen et al., 2003; Marlin et al., 2017). However, recent studies showed that significant amounts of glacier ice are located below the sediment-mantled slopes, yielding a 10 % uncertainty on the glacier area (Bernard et al., 2014, 2024). The present-day glacier is constrained by alpine mountain peaks, such as Slåttofjellet (580 m a.s.l.), Haavimbfjellet (783 m a.s.l.), and Nobilefjellet (876 m a.s.l.) and the proglacial area in the north (Fig. 1).

The slopes of the Austre Lovénbreen basin are composed of steep rock walls in the upper section and unconsolidated angular debris formed by paraglacial erosion processes in the lower section, which were glacially reworked in several areas. These loose slope sediments adjust to their natural slope angle, ranging from 38 to 42°.

Geologically, the Austre Lovénbreen basin is located in the Kongsvegen group, situated along the northernmost part of the Tertiary fold and thrust belt of western Spitsbergen, accompanied by several north-south striking faults and characterised by nine NE- to NNE-vergent thrust sheets (Barbaroux, 1967; Bergh et al., 2000; Hjelle et al., 1999; Saalmann and Thiedig, 2001, 2002). The Kongsvegen group consist of low to medium grade metamorphic rocks, including mica schists interlayered with marble, quartzite or gneisses (Bogegga Formation), the greyish to yellowish dolomite marbles (Steenfjellet Formation) and phyllites with quartzite layers (Nielsenfjellet Formation) (Hjelle et al., 1999).

Located at 78°N, the study site is characterised by a high arctic maritime climate (Eckerstorfer and Christiansen, 2011). The North Atlantic current moderates the temperature at Svalbard compared to other regions at the same latitude (Maturilli et al., 2019). The snow cover period typically extends from September or October until June. The average annual precipitation in Ny-Ålesund is around 470 mm, with a peak of monthly precipitation in autumn and winter. However, over the past few decades, there has been a documented increase in both the total precipitation and the frequency of heavy rainfall events (Førland et al., 2011; Maturilli et al., 2019). On average, precipitation levels have risen from 427.7 mm during the period from 1980 to 2000 to 511.4 mm between 2000 and 2020, representing a 19.7 % increase (Fig. 2). The recent temperature increase due to global warming has been more pronounced around Svalbard than anywhere else on Earth (Nordli et al., 2014; IPCC, 2021). The mean annual air temperature (MAAT) in Ny-Ålesund increased from −5.7 °C between 1980 and 2000 to −3.6 °C between 2000 and 2020 (Fig. 2).

3. Material and methods

3.1. Lidar data acquisition and processing

Terrestrial lidar data acquisition was performed annually from 2012 to 2018 and twice in 2021 using a Riegl LMS-420i (2012), a Riegl LPM-321 (2013–2015) and a Riegl VZ-6000 (since 2016) (RIEGL, 2010a, 2010b, 2016). TLS campaigns in 2019 and 2020 were impossible due to difficult pandemic restrictions. Two campaigns were conducted in 2021, capturing the pre-failure (e.g., no observable slope failures; 2021-1) and the post-failure state (2021-2). The technical upgrade of the utilized equipment has followed the overall improvement of available terrestrial lidar technology since 2012, increasing overall performance (e.g., range, beam divergence, resolution, measurement speed) (Telling et al., 2017). The increased range of the Riegl VZ-6000, allowed the implementation of additional scan positions (e.g., Haavimbfjellet peak). Since 2016,

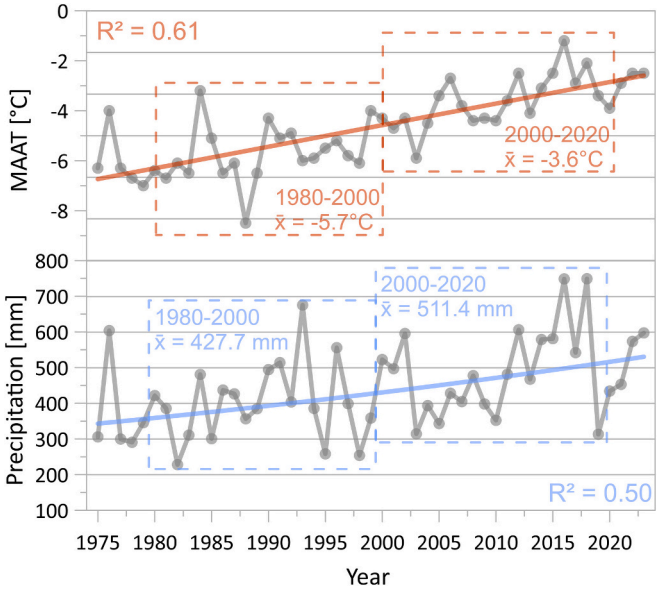

Fig. 2. Annual Precipitation (blue) and Mean Annual Air Temperature (red) in Ny-Ålesund from 1975 till 2023.

monitoring almost the entire glacier basin (>95 %) has been possible, whereas previous scans were only conducted in the context of individual slopes. Data gaps result from occlusions (e.g., crevasses, meltwater channels) and meltwater on the glacier surface (e.g., laser beam absorption) (Prokop, 2008; Abellán et al., 2014). Referenced colour images were acquired by the internal camera of the VZ-6000 or a calibrated high-resolution digital camera mounted on the respective laser scanners. The data acquisition was performed at the end of the ablation period and in sync with the measurement of the ablation stakes (Friedt et al., 2012) installed on the Austre Lovénbreen glacier.

More than 300 scans from 13 different scan positions were carried out, resulting in point cloud resolutions between approx. 0.05 m and 0.40 m within the study site (approx. 0.05 m to 0.20 m at the sediment-mantled slopes). Georeferencing, fine registration of individual laser scans and subsequent multi-temporal registration was done using an ICP algorithm implemented within the Riegl RiSCAN Pro software (Chen and Medioni, 1991; Besl and McKay, 1992; RIEGL, 2013). A reference point cloud, derived from an available 5 × 5 m Digital Elevation Model (DEM) in UTM coordinates (EPSG:25833), was used for geo-referencing the TLS data (NPI, 2014). The DEMs used in the further distance change analysis were derived for every TLS campaign from the registered and geo-referenced point clouds within CloudCompare with a resolution of 0.25 × 0.25 m (CloudCompare, 2021). Interpolation of the data was not performed to avoid the introduction of errors. After pre-filtering non-ground points using automated filter solutions (e.g. bare earth filter, Hove-Wedge, etc.) we primarily filtered manually due to the complexity of the terrain to improve results for generating DEMs (Panholzer and Prokop, 2013, 2018; Rieg et al., 2014; Wichmann, 2015).

3.2. Mapping and volume calculation

Analyses of terrain changes were investigated through DEMs of Difference (DOD) created with the software Geomorphic Change Detection 7.4.1.0 (Wheaton et al., 2010) and diffuse hillshades created with the ambient occlusion method implemented in SAGA GIS (Tarini et al., 2006). A spatially variable level of detection with a confidence interval of 95 % (LOD95%) was calculated to differentiate between real changes and data noise (Prokop and Panholzer, 2009; Lague et al., 2013; Fey and Wichmann, 2017). Debris slides and debris flows were mapped based on the DOD and hillshades and validated by field surveys. The results were used as Areas of Interest (AOI).

Several debris slides had their runout onto the glacier. Thus, it was not possible to quantify the accumulation zone as the exact elevation of the glacier surface during individual sliding events could not be determined. Therefore, the volume of each debris slide was investigated using AOI masks of the zone of depletion as defined by Cruden and Varnes (1996) to reduce uncertainties in the qualitative analysis and avoid quantifying the adjacent glacier ice volume changes.

Quantification of erosion and deposition caused by snow avalanches could not be quantified due to their limited impact (below LOD95%; <5 cm on the slopes) and due to the lack sediment traps, which would likely fail in the extreme environment. Additionally, snow avalanche entrainment paths could not be identified in the TLS data even after a 10-year period. Thus, the utilized methods are inadequate for quantifying the erosional rates of snow avalanches.

3.3. Automated camera system monitoring and image analysis

A comprehensive investigation of causal relationships between meteorological conditions and the spatial and temporal occurrence of debris slides within the Austre Lovénbreen basin requires higher temporal resolution than annually performed TLS measurements. Hence, the network of autonomous cameras (Fig. 3) from the long-term observatory project monitoring the Austre Lovénbreen since 2007 was utilized (Bernard et al., 2013; Friedt et al., 2023). This network provides a surface coverage of 96 % of the glacier and the adjacent slopes. Thus, the date of failure, triggering mechanisms and temporal evolution of individual debris slides could be investigated, provided that visibility was

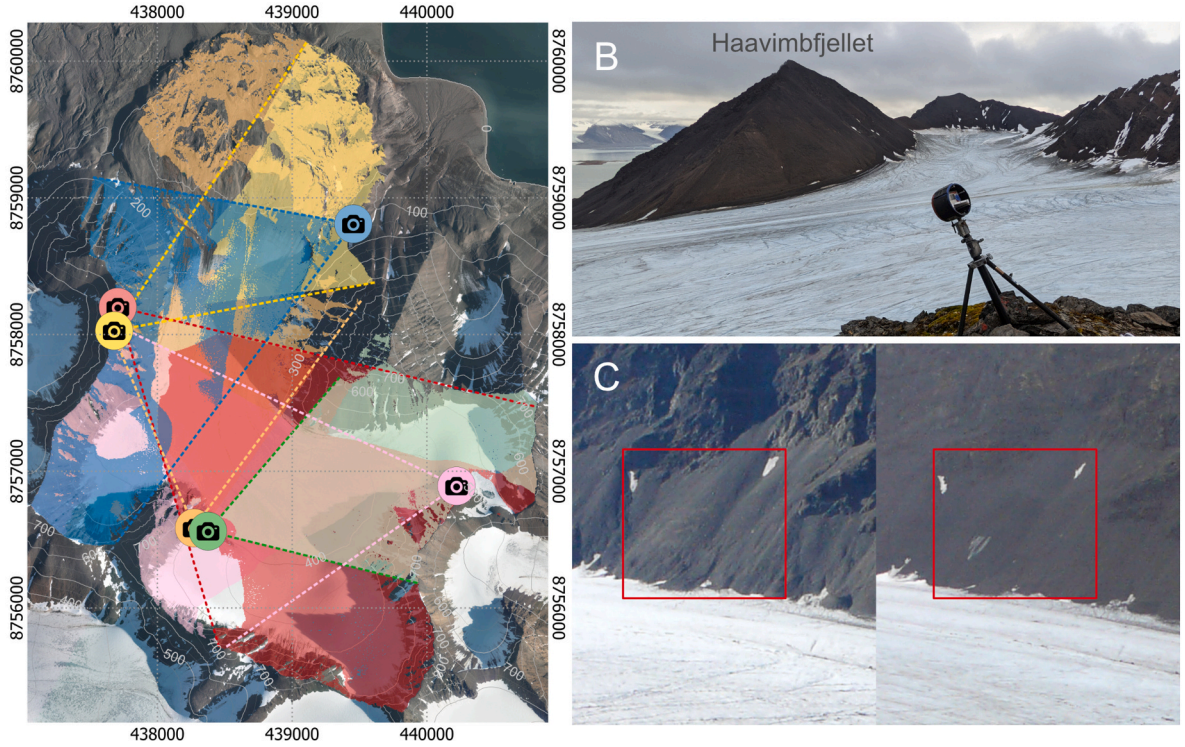

Fig. 3. Automated camera system monitoring within the Austre Lovénbreen basin. A) Locations of the autonomous cameras with their individual viewshed. B Camera setup is located on a ridge southwest of the glacier basin. C) Examples of pictures taken by the northernmost automated camera system before (left; 14.08.2015) and after (right, 16.08.2015) a small debris slide located on Slåttofjellet.

not limited by poor weather. Furthermore, the identification, dating and quantification of debris slides and debris flow occurring in the years 2019 and 2020 was done by the available camera images. An additional TLS campaign in early 2021, before any seasonal debris slide activity occurred, allowed mitigating data gaps in the time-series. Furthermore, the camera data allowed for a qualitative analysis of debris slide activity since 2007 within the Austre Lovénbreen basin, extending the observation period by five years.

The cameras provided up to three images per day depending on the polar sun cycle and meteorological boundary conditions. Typical for systems installed in such harsh conditions, data gaps are associated with temporary system or data storage failure (Bernard et al., 2013). Analysis of the >53,500 images was done manually, as the image's resolution for the different slopes, combined with lighting and contrast variations, did not allow for an automated analysis. Due to insufficient image resolution, the identification of debris slides and debris flows on slopes with large distances to the cameras (>1000 m) was limited to events >100 m^3.

Furthermore, the automated camera network allowed for a visual qualitative assessment of avalanches as several hundreds of snow avalanches could be observed during the spring, which commonly showed to entrain debris from the slopes.

3.4. Meteorological data

In this study, meteorological data from two stations were used: I) the airport meteorological station in Ny-Ålesund 8 m a.s.l., roughly 5 km east of the Austre Lovénbreen basin (MET Norway, 2024); and II) an IPEV Automatic Weather Station located on a ridge southwest of the glacier basin, approx. 450 m a.s.l. (Bernard et al., 2013).

All meteorological variables used in this study were based on hourly measurements of air temperature and precipitation. MAAT and freezing degree days (FDD) were calculated for the hydrological year, defined from 1 October to 30 September, to encompass the entire snow season. The cumulated thawing degree days (TDD) were calculated for full calendar years or till the failure date of a specific debris slide (TDD @ failure), as the main energy source is solar radiation during summer (Christiansen et al., 2013). In addition to the observation sites, FDD and TDD were also calculated for different altitudes based on the daily average temperature gradient between Ny-Ålesund and the On-Site station.

Cumulative precipitation parameters were calculated for the hydrological year and the hydrological summer (1 May to 30 September) to further investigate the influence of rainfall events in the summer without considering the large quantities of snow falling during the winter months. In order to assess the influence of heavy precipitation events, the cumulative squared daily precipitation (Cum. Precipitation^2) was used. Daily precipitation data is squared and consequentially summed up for the entire hydrological summer (Cum. Precipitation$^2_{hs}$, mm^2) or till the failure date of a debris slide (Cum. Precipitation$^2_{hs}$ @ failure, mm^2), assuring that higher rainfall intensities have a higher impact on the statistical analysis than represented by the cumulative daily precipitation as shallow planar debris slides are frequently triggered by extreme rainfall (e.g. Hungr et al., 2014; Peruccacci et al., 2017).

4. Results

4.1. Debris slide formation and characterisation

The Haavimbfjellet and Slåttofjellet primarily comprise low-strength and penetrative foliated phyllites of the Nielsenfjellet Formation, which act as the main source area for rock falls (Fig. 1 A). No indications of deep-seated landslide phenomena (e.g. tension cracks, graben, uphill facing scarps) within the Austre Lovénbreen basin could be identified, as commonly found in similar lithology (Agliardi et al., 2001; Macfarlane, 2009; Zangerl et al., 2010). Sediment-mantled slopes can be observed beneath the steep rock slope sections, reaching either pro-glacial till deposits or the current glacier surface, which are reworked by debris flows, translational debris slides, and snow avalanches in the winter and spring. The slope angle of the sediment-mantled slopes varies between 34 and 40°. Areas of intense avalanche activity or debris flow activity, on average lead to gentler slope angles than sections predominantly formed by rock falls due to their longer runouts on the glacier (De Haas et al., 2015; Tomczyk, 2021).

Sparse rock screes or individual rocks deposited by snow avalanches extent from the slopes onto the glacier surface, but the quantification of the erosional capabilities of snow avalanches on the slopes was not possible with the current data set due to their limited impact on the slopes (below LOD95%). The deposition of debris through avalanches on the glacier could not be identified within the TLS data as the amount of the deposited material found on the glacier during the field campaigns was marginal compared to the dominant loss of glacier ice, which exceeded sediment deposition by up to two orders of magnitude. Thus, the limited deposition of debris via avalanches on the glacier surface had no discernible impact on the ablation of the glacier.

In the sediment-mantled slopes, a distinct subsurface ice layer is observed in the Austre Lovénbreen basin, temporarily exposed after a slope failure (Fig. 4). Thus, the extent of the ice layer could be mapped in areas of debris slide activity, and additional data about the scree thickness could be derived from DODs. GPR measurements by (Bernard et al., 2014, 2024) have shown that the thickness of the ice layer can reach up to several meters and is connected to the glacier.

This subsurface ice layer could also be found on sections of the talus slopes with no visible connection to the glacier since the 1970s and extends to a height up to 140 m above the present glacier elevation.

Translational debris slides, and to a lesser extent debris flows, dominated the recent surface evolution of the slopes found within the Austre Lovénbreen glacier catchment during the observation period (Fig. 4). However, the impact of these processes and sediment flux changes significantly from North to South. The sediment-mantled slopes can be therefore divided into three sections: I, II, and III.

Section I is located beyond the extent of the lateral moraines of the Austre Lovénbreen and Midtre Lovénbreen (Fig. 5). The foot of the slope has not been glaciated during the maximum extent of the LIA in 1920s, as seen in aerial photographs. The predominant agents of sediment transport during the observation period were debris flows ($n = 11$), also indicated by the much gentler slope angles (33–37°) found in Section I as opposed to anywhere else observed within the study area. Furthermore, the talus slopes are deeply incised by debris flow channels, which are often framed by levees. No debris slides ($n = 0$) have been observed within this area, and no indication of debris slide deposits could be found.

Section II has experienced gradual deglaciation since the 1970s, as seen in Marlin et al. (2017). Translational debris slides ($n = 18$) and, to a lesser extent, debris flows ($n = 4$) dominate this section. The debris flows occurred during the observation period only in the upper section of the talus slopes without reaching the valley floor (Fig. 5). However, older debris cones with distinct debris flow channels and levees are located within this section.

Section III comprises talus slopes in contact with the retreating glacier. The talus is dominated by translational debris slides ($n = 129$). Runout lengths of up to 25 m (Figs. 4B & 6C) could be observed forming lobate debris slide deposits. Limited debris flow activity ($n = 6$) was observed, which was responsible for <2 % (Fig. 8 & Table 1) of the total sediment flux.

4.2. Debris slide kinematics

The translational debris slides observed within the study site are characterised by a rupture surface formed at the contact zone between the talus scree and the subsurface ice layer.

Due to the similarity regarding the kinematics of the observed debris

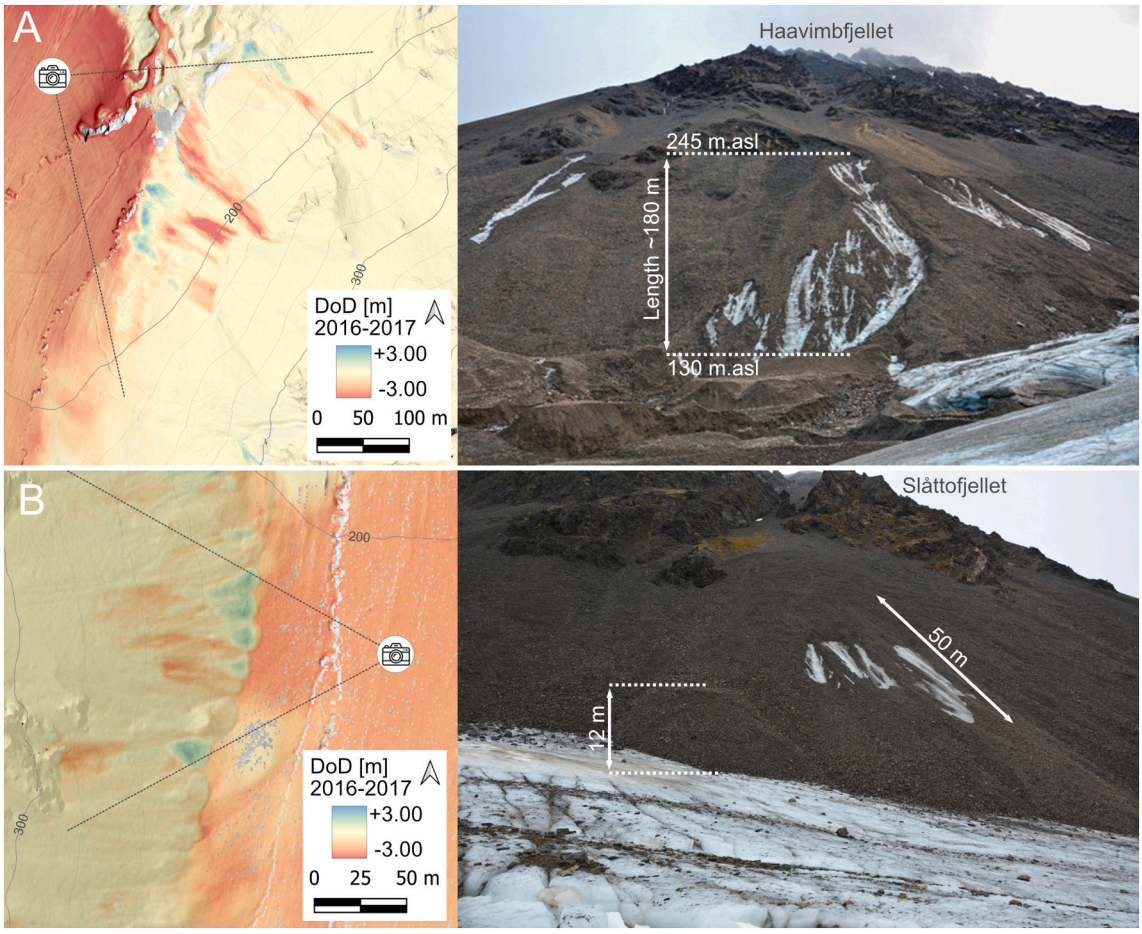

Fig. 4. DEMs of Difference (TLS data: 2016/2017) and corresponding photographs of debris slides in 2017. Scarps of the debris slides are visible in the DODs, with red colours uphill corresponding to debris ablation and blue colours downhill corresponding to debris accumulation. A) Several debris slides at the snout of the glacier looking upward towards Haavimbfjellet in 2017, triggered by heavy rainfall. The sub-surface ice layer is exposed up to 115 m above the glacier surface. B) Debris slide at the slopes of Slåttofjellet triggered without any rainfall.

slides, it was possible to identify five phases of debris slide induced slope evolution. The slope along Profile A-A' (Fig. 6B) has been chosen to visualise the ongoing slope processes through a documented representative example as high-resolution TLS data since 2014 is available, and no previous slope failure could be identified. Schematic cross-sections (Fig. 7) are based on the TLS data. However, the thickness of the sediment layer, debris slide deposits, subsurface ice layers and the ablation of the glacier are exaggerated within the model by a factor of 1:2 to allow for better visibility. The initial pre-failure topography (TLS 2016) and the 1936 topography (Girod et al., 2018) have not been altered to preserve the original slope angle and provide a conformal representation of the morphology of the pre-failure slope.

Phase 1 depicts the typical sediment-mantles (pre-failure) slope system within Section III. The upper section is characterised by steep rock walls consisting of low-strength phyllites with quartzite interlayers (S166/34) with scree deposits below extending onto the glacier until a thin veneer of rock fall and snow avalanche deposits remains. The glacier has lost roughly 55 m in elevation between 1936 (Girod et al., 2018) and 2016. Furthermore, previous studies have shown that a significant amount of glacier ice continues below the current extent of the talus (Bernard et al., 2014, 2024). Field observations after several slope failures indicate the presence of a sub-surface ice layer (Fig. 4) at least to an elevation of 299 m a.s.l., which is approximately 94 m above the glacier level in 2016 at this position.

Phase 2 is characterised by a rapid first-time failure followed by retrogressive sliding above the main scarp. On 27.08.2017, a translational debris slide occurred at profile A-A' as the sub-surface ice layer was exposed. Retrogressive sliding above the main scarp started soon after, until the exposed ice layer was covered with sediment within approximately five weeks (until 06.10.2017). The primary debris slide deposit had a volume of 3181 $\pm$ 318 m^3 with a runout length of roughly 8 m onto the glacier surface, which formed a lobate tongue-shaped deposit. The maximum scarp height was approximately 4.20 m.

The slope failure occurred after a two-week period of increased air temperatures, with daily maxima reaching up to 11.3 °C in Ny-Ålesund three days prior. Limited rainfall was observed within the two weeks prior to the slope failure.

Phase 3 corresponds to the slope readjustment after a debris slide during winter and spring (06.10.2017 until 08.07.2018 for the schematic cross-section) through the continuous retrogressive failure of the main scarp and snow avalanches in the winter, the morphological features of the main scarp are overprinted. Furthermore, an increased creep of areas above the debris slide scarp could be observed within the TLS data utilising an IMCORR approach (Fahnestock et al., 1992; Scambos et al., 1992).

Phase 4 comprises two main processes: I) the secondary debris slide, occurring above the initial debris slide, and II) the readjustment of the debris slide deposit on the glacier. Secondary debris slides can be commonly (08.07.2018 at Profile A-A') found with the Austre Lovénbreen basin triggering above the initial debris slide. The interval between two consecutive events can take several years, depending on the meteorological boundary conditions. Lateral and frontal toe collapse

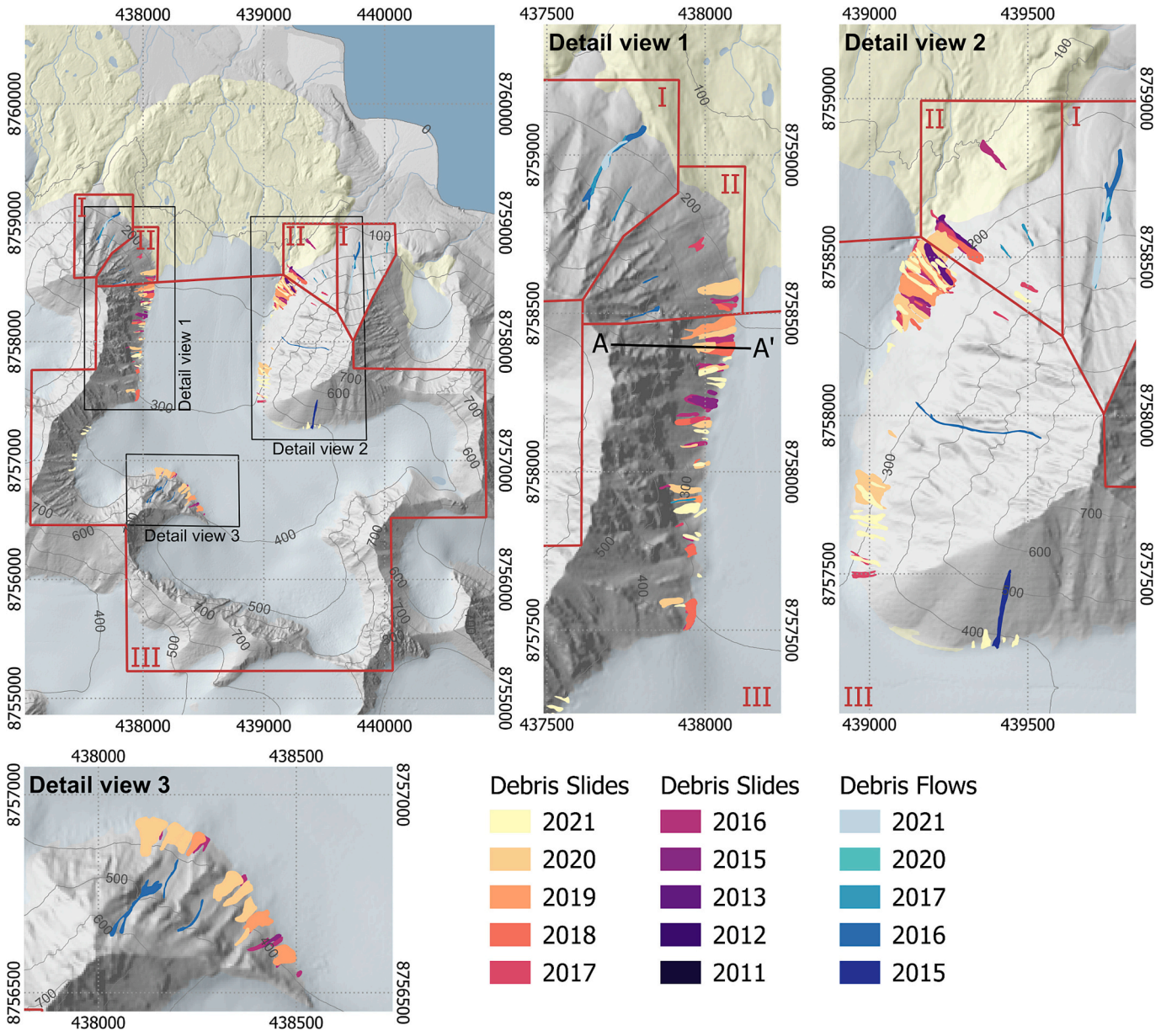

Fig. 5. Overview of all observed debris slides and debris flows from 2011 to 2021 within the Austre Lovénbreen basin. The slopes were differentiated depending on the dominant process (Sections I, II, and III, indicated in red). Profile A-A' is indicated within Detail View 1.

of the initial debris slide deposit was observed, leading to a steep crest and a small talus apron in front of the main debris slide deposit, forming a morphology which is similar to a small talus-derived rock glacier (Fig. 7, Phase 3). No height change was measured by TLS at the top of the deposit, indicating that the debris slide material has neither settled nor that the glacier ice below has melted. Thus, the debris slide deposits protect the glacier from further ablation.

Phase 5 corresponds to the long-term adjustment of the sediment-mantled slope towards a stable equilibrium. Continued loss of glacier ice has led to additional frontal and lateral toe collapse of the debris slide deposit at the base of the slope. Underneath this deposit, the buried glacier ice is preserved according to the thickness of the scree material above, forming a steep sediment apron (Fig. 7, Phase 5, Detail view). The sediment-mantled slope further adjusts to the new slope angle defined by the debris slide deposit.

At Profile A-A' from the debris slide deposit, a scree apron with a height of approximately 5 m and a thickness of 40 cm had formed after four years. The top of the debris slide deposit has settled at the crest by a maximal 0.3 m within three years and can be considered stable. The largest debris slides (e.g. longest runout lengths) located on the glacier may show flow features after several years, as the glacier ice drags the deposit along the main flow direction. Thus, larger deposits may bear strong morphological similarity to small protalus rock glaciers, except for a core of glacier ice. Debris slide deposits show no measurable creep if located beyond the extent of the Austre Lovénbreen glacier.

4.3. *Magnitude and frequency of debris slides and debris flows*

During the observation period, 171 distinct events could be identified. These encompass 147 translational debris slides, 21 debris flows and 3 rock falls (>1 m^3). Smaller rock fall events were commonly observed during the field campaigns, but individual events could not be differentiated via the TLS data. Debris slides were responsible for approx. 96 % ($V_{Debris\ Slides}$: 122889 ± 6109 m^3) of the entire sediment flux observed at the slopes of the Austre Lovénbreen basin (Table 1). Thus, debris flows act as a minor agent of sediment transport (V_{Debris}

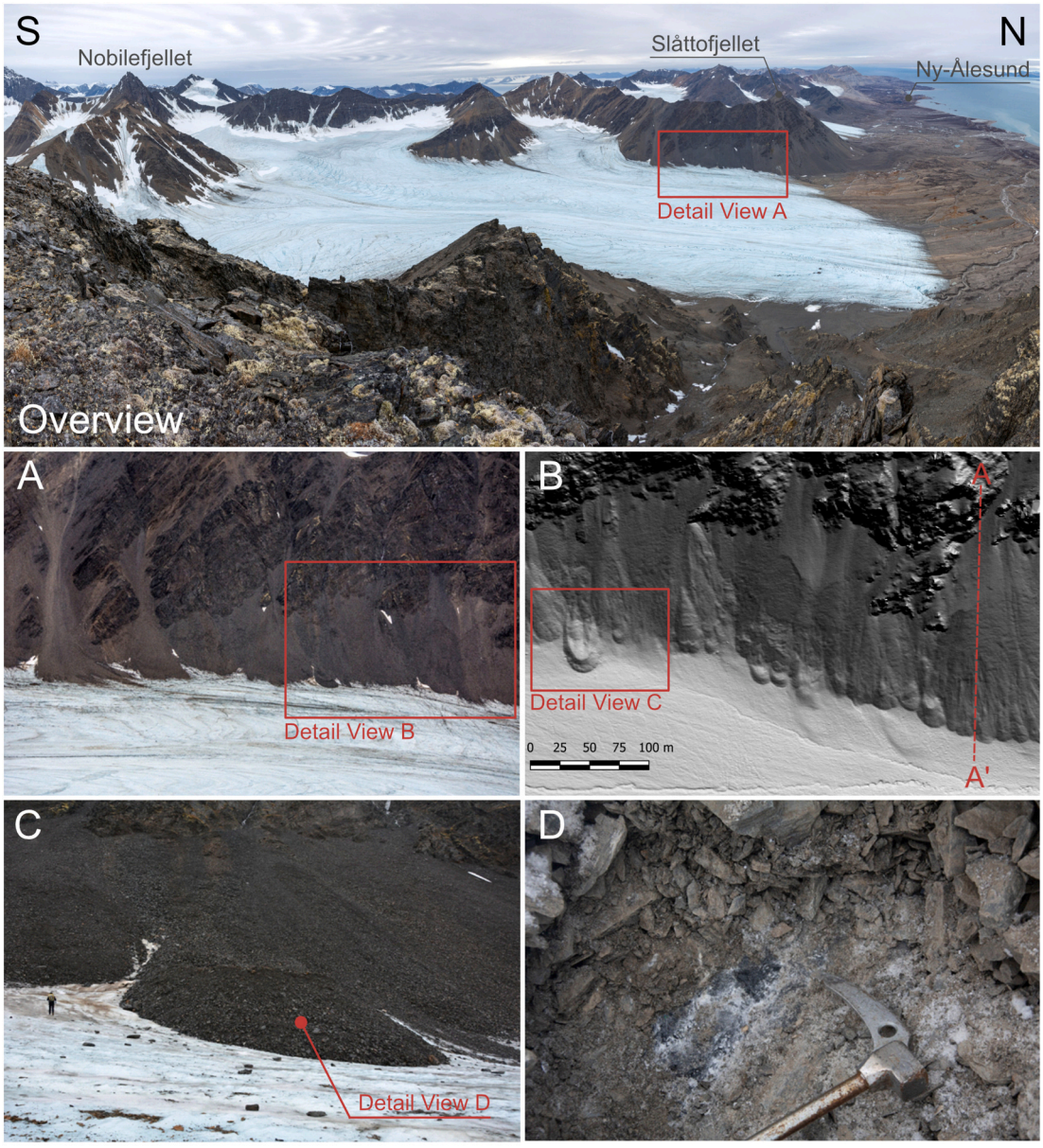

Fig. 6. Overview of the Austre Lovénbreen glacier from the summit of Haavimbfjellet with cascading detail views; peaks and Ny-Ålesund are indicated. A) Photograph of the talus slopes of Slåttofjellet adjacent to the glacier. B) Hillshade of the 2017 TLS, Profile A-A' is indicated; C) Photo of the largest debris slide deposit found within the study site; person for scale. The camera system documented the initial failure in 2010. D) Trench at the front of the debris slide deposit. A solid ice core could be found after approximately 40 cm.

Table 1
Debris slide and debris flow volume, area and quantity observed between 2011 and the TDD, cumulative daily precipitation for the hydrological summer (Cum. P_{hs}) and cumulative daily squared precipitation for the hydrological summer (Cum. P^2_{hs}). Debris slide volumes have been calculated using a spatially variable LOD (confidence interval of 95 %).

Year	Debris slide area [m^2]	Debris slide volume [m^3]	n	Debris flow area [m^2]	Debris flow volume [m^3]	n	TDD [°C]	Cum.P_{hs} [mm]	Cum.P^2_{hs} [mm^2]
2011	8526	No Data	4	0	0	0	630	148	1023
2012	4522	1828 ± 228	2	0	0	0	545	135	1120
2013	12946	7943 ± 638	3	0	0	0	553	264	2381
2014	0	0	0	0	0	0	449	242	2769
2015	14716	6446 ± 802	8	3824	552 ± 110	1	616	166	1507
2016	36853	15474 ± 1719	36	18605	2445 ± 328	8	687	243	3667
2017	28373	18407 ± 1202	15	8970	1064 ± 194	9	649	220	3943
2018	31151	20558 ± 1440	13	0	0	0	624	269	3912
2019	23910	3172 ± 367	4	0	0	0	595	126	779
2020	74571	42525 ± 5563	27	0	0	0	729	143	856
2021	35235	6829 ± 1308	39	6050	920 ± 255	3	547	152	1991

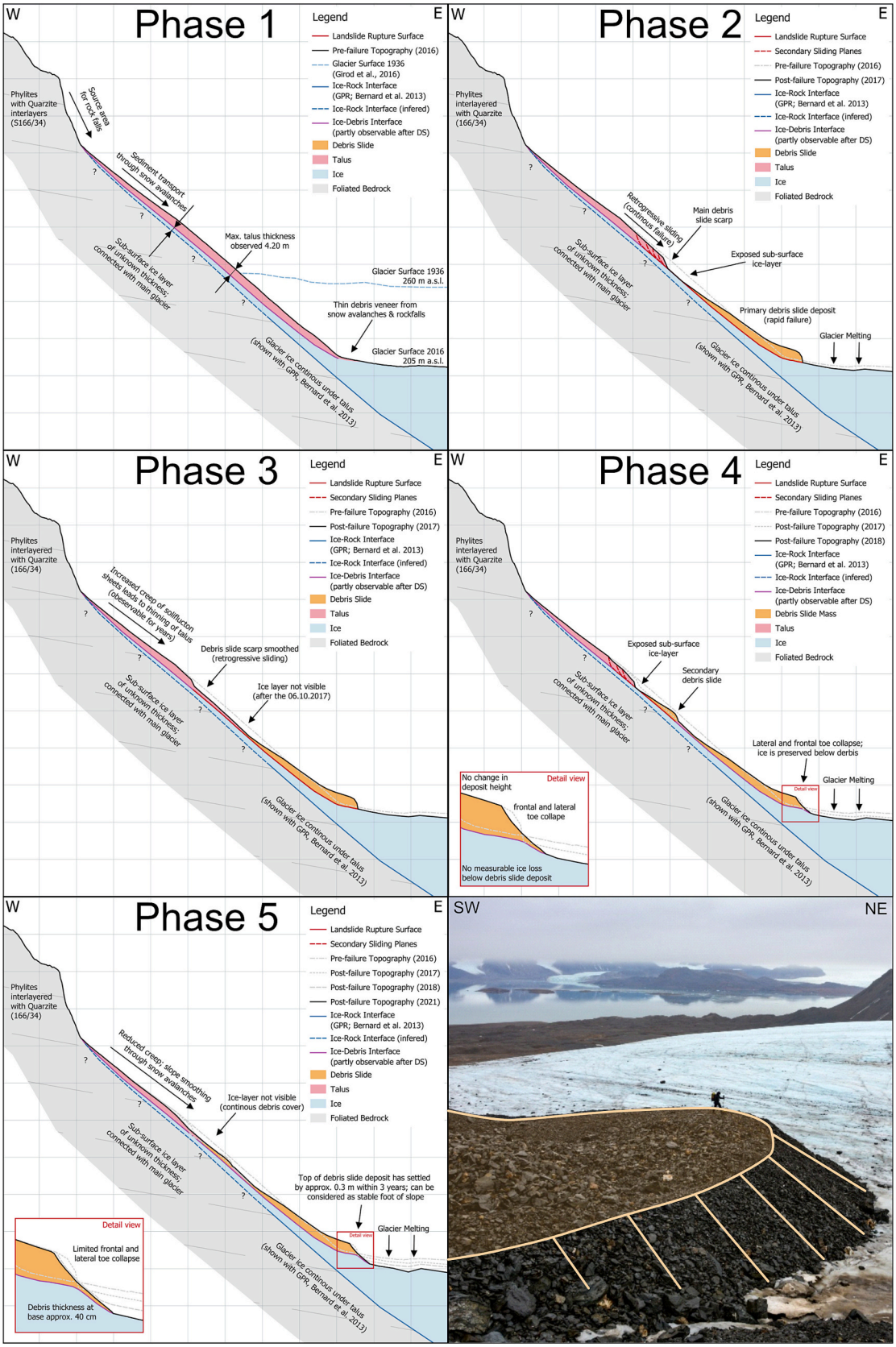

Fig. 7. Schematic cross-sections depicting the slope evolution at Profile A-A' between 2016 and 2021 with an example picture of the largest debris slide deposit within the Austre Lovénbreen basin. Phase 1) State of the pre-failure slope found in 2016. Phase 2) Initial translational debris slide, exposing the sub-surface ice layer. Phase 3) Slope readjustment through the continuous retrogressive failure of the main scarp. Phase 4) Secondary translational debris slide. Lateral and frontal toe collapse of the initial debris slide deposit. Phase 5) Long-term adjustment of the sediment-mantled slope towards a stable equilibrium. Continued loss of glacier ice has led to frontal and lateral toe collapse of the debris slide deposit. The buried glacier ice is preserved underneath the debris.

$_{Flows}$: 4982 ± 631 m^3), except within Section I (Fig. 5).

The observed debris slides vary strongly in volume, extent, and depth throughout the years, with debris slides ranging from 12 ± 5 m^3 to 9296 ± 503 m^3 with an average volume of 836 m^3 and debris flows from 19 ± 5 to 996 ± 107 m^3 with an average volume of 237 m^3 (Fig. 8). However, there is a strong correlation between the area and volume of debris slides due to the subsurface ice layer acting as the rupture surface (Fig. 8, right).

The frequency and magnitude of individual debris slide events greatly fluctuate within the observation period (Fig. 8, left). However, a significant increase in the overall debris slide activity (R^2 = 0.57; *P*-Value = 0.0068) can be observed between 2011 and 2021 (Fig. 9).

4.4. Impact of meteorological parameters on debris slide initiation

Through the camera network, the date of failure of 106 translational debris slides could be identified within a range of hours or days, depending on the visibility (e.g., clouds, fog, excessive rain).

The time of failure for the observed debris slides ranges from late August till the beginning of October (Fig. 10), when the maximum thaw depths are reached. However, a few events could also be observed in the lower altitudes during July. No in-situ data for the thaw depth was available within the slopes. Thus, the annual maximum thawing degree days measured in Ny-Ålesund (TDD) serve as a proxy value to quantify the overall heat input during the year projected onto the entirety of the Austre Lovénbreen basin (Fig. 11). The majority of precipitation at Ny-Ålesund during the hydrological year falls during the winter period as snow. Thus, the cumulative precipitation during the hydrological summer is better suited to quantify the impact of precipitation on debris slide formation within the Austre Lovénbreen basin (Fig. 11).

A general trend between debris slide volume and meteorological boundary conditions can be observed for individual debris slide events. Higher temperatures (TDD @ failure) and rainfall intensities (Cum. $Precipitation^2_{hs}$ @ failure) observed during the years lead to larger debris slides. Furthermore, a cluster of primary temperature-induced debris slides occurring in 2020 can be observed (Fig. 12).

When analysed per year, a strong correlation (R^2 = 0.94) between the cumulative squared daily precipitation ($Rainfall^2$ hydro. summer) and the total debris slide volume per year could only be found when temperature outliers were not considered (Fig. 13). Since 2007, a TDD of at least 545 °C had to be reached for any debris slides to occur, indicating a thermal threshold necessary for debris slide formation within the Austre Lovénbreen basin beyond heavy rainfall events (Fig. 14). This is outlined from 2007 till 2010 and 2014, when no debris slides were observed (Fig. 15), even though a potentially sufficient amount of rainfall was given (Fig. 13). Thus, a temperature threshold necessary for heavy rainfall events to trigger an initial slope failure can be assumed. Furthermore, as in 2020, debris flows occurred without observable rainfall prior to the slope failures (meteorological stations; automated camera network) beyond a TDD of 700 °C.

Ultimately, the best description of the increase in debris slide magnitude is achieved for all data points (2012-2021) with a linear model that includes both temperature (TDD) and heavy rainfall (Cum. $Precipitation^2$hs) variables (Fig. 16). The negative interaction term shows that the effect of temperature and rainfall variables is less than the sum of the individual effects.

5. Discussion

5.1. Data limitations

Particular advantages and deficiencies of the applied remote sensing techniques became evident in our study. The multi-temporal TLS data allowed us to detect and quantify incremental terrain changes between individual TLS campaigns within a distance-variable LOD95%. However, the limited temporal resolution of TLS (i.e. one measurement per year) does not provide sufficient information to investigate the trigger mechanisms of slope processes. The automated camera network's main purpose was to evaluate snow cover in the most remote and inaccessible areas (Bernard et al., 2013; Friedt et al., 2023), it proved particularly effective for qualitative debris slide and debris flow detection and provided key information about the failure date, duration, trigger mechanisms, and kinematics of debris slides, while increasing the observation period by five years. Data gaps within the TLS data could also be amended as the failure dates of almost all large translational debris slides (>2000 m^3) could be identified within the photographs. Thus, the temporal limitations of the TLS data were reduced significantly.

While it was possible to identify the event time of 106 translational debris slides (n = 147), only 7 debris flows (n = 21) and no rock falls could be identified. This is unsurprising due to the differences in the

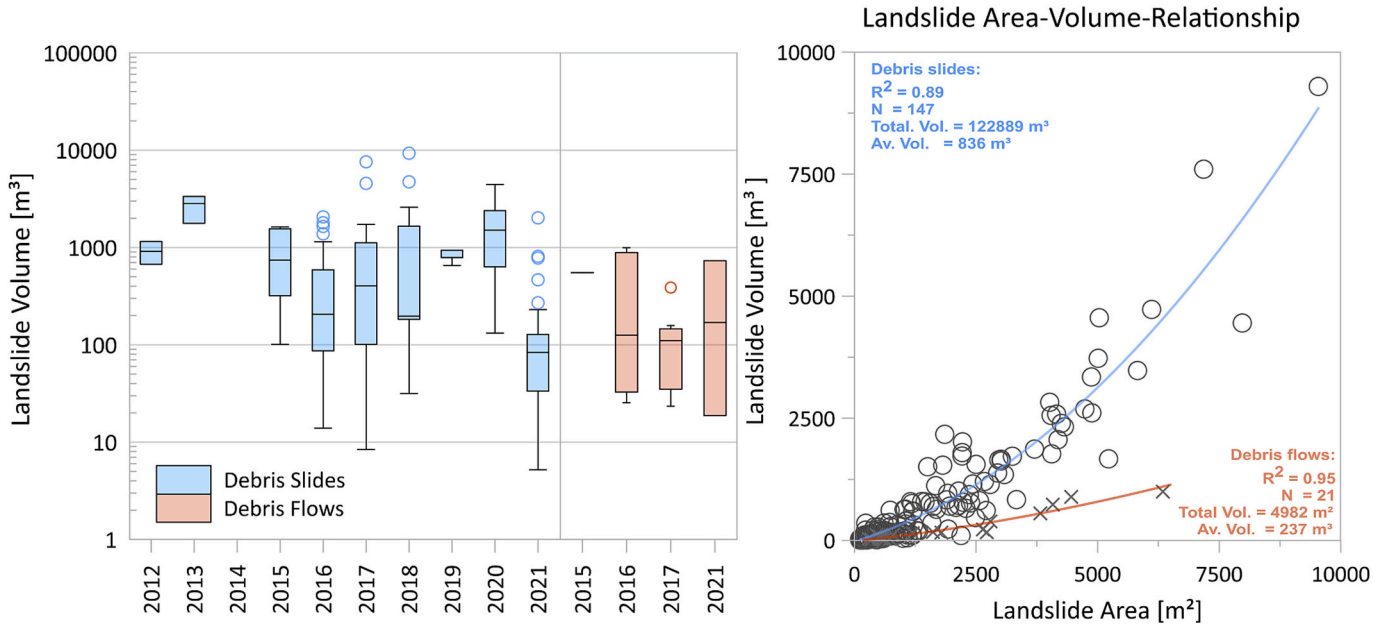

Fig. 8. Boxplot of all observed debris slides and debris flows per year (left) and the are-volume relationship for both processes (right).

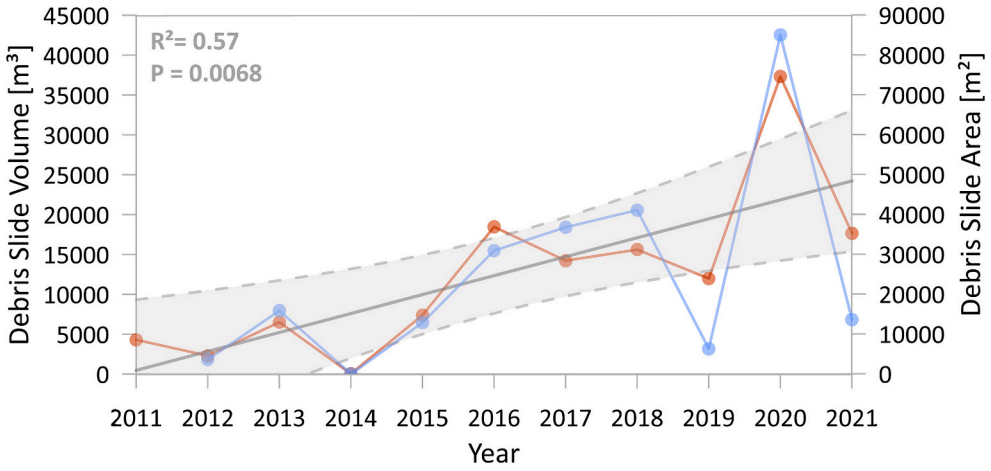

Fig. 9. Total Debris slide area (red) and volume (blue) per year observed within the Austre Lovénbreen basin. Linear fit with a 95 % confidence interval for the debris slide area is indicated in grey.

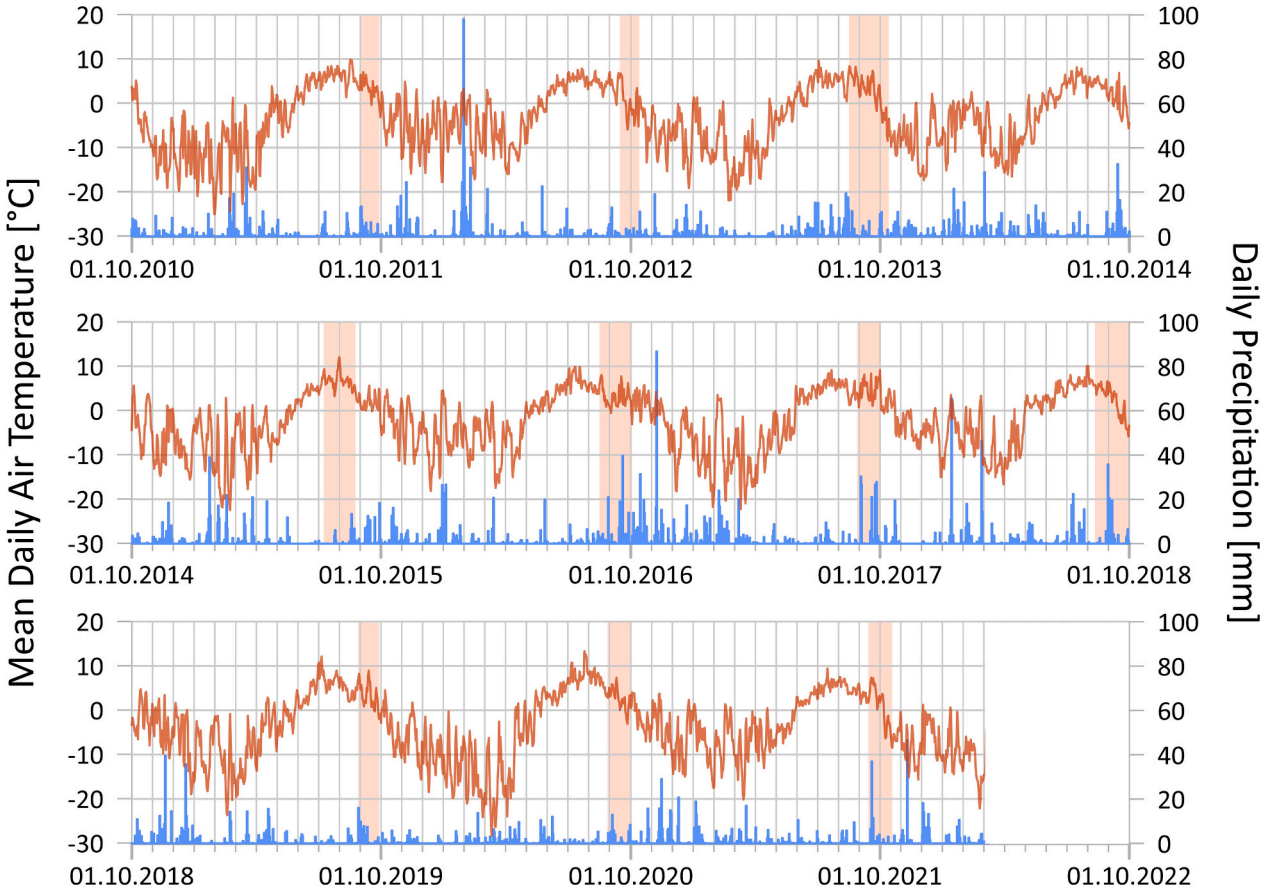

Fig. 10. Daily mean air temperature and daily precipitation at the Ny-Ålesund meteorological station from 2010 to 2021. Periods of observed debris slide activity are indicated in red.

average volume between the debris flows and debris slides (Fig. 8). Whereas small-scale debris slide events ($\leq$100 m^3) at larger distances from the cameras are often difficult to detect, it must be emphasized that the network was originally not designed for this task. Furthermore, the 49 small-scale events ($\leq$100 m^3) between 2012 and 2021 only accounted for approx. 2 % of the total sediment flux. This may introduce certain data biases within the investigation of trigger mechanisms and magnitude on an individual level (Fig. 12), but does not affect the statistical analysis of the annual debris slide activity (Figs. 13, 14 & 16). The identification of landslide processes prior to available TLS data based solely on the automated camera network as the ALS-Data from 2010 (NPI, 2014) proved insufficient to quantify debris slides. Thus, only the areas of the four translational debris slides in 2011 were mapped (Table 1).

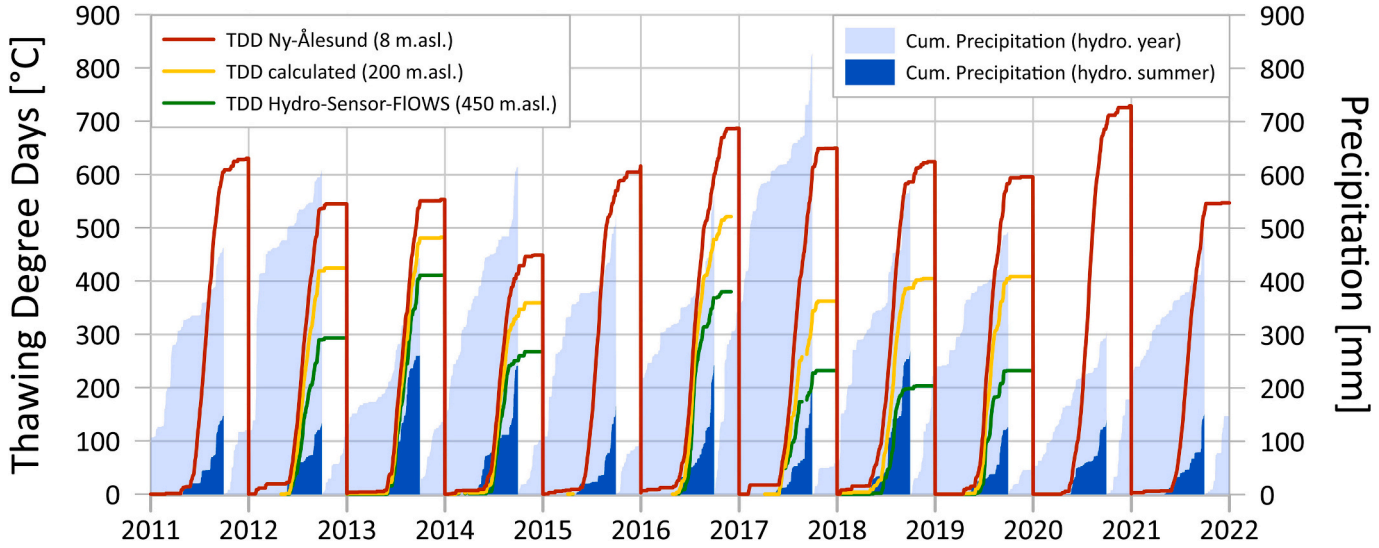

Fig. 11. Thawing Degree Days measured at Ny-Ålesund (8 m a.s.l.), the IPEV Automatic Weather Station within the Austre Lovénbreen basin (approx. 450 m a.s.l.), and a TDD calculated exemplary for 200 m a.s.l. based on the height-dependent temperature gradient of the available datasets and the cumulative precipitation for the hydrological year and summer.

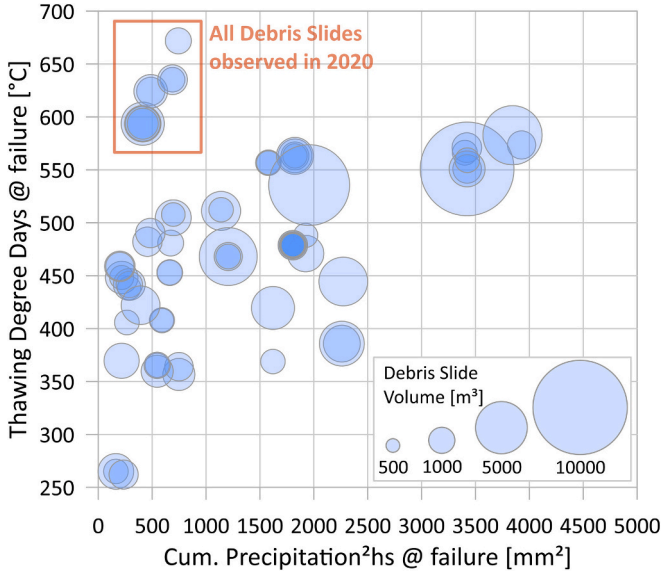

Fig. 12. Thawing degree days (TDD @ failure) and cumulative squared daily precipitation during the hydrological summer (Cum.Precipitation$^2_{hs}$ @ failure) were calculated for the date of the initial slope failure of 106 individual debris slides observed between 2011 and 2021.

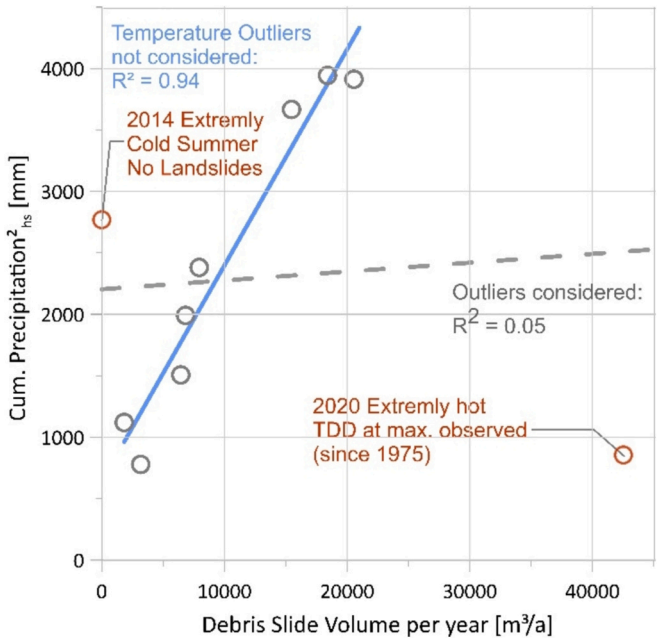

Fig. 13. Impact of rainfall on debris slide formation. Cumulative squared daily precipitation (hydro. Summer) and debris slide volume per year between 2011 and 2021.

5.2. Spatial extent and origin of sub-surface ice layer within the sediment-mantled slopes

Reconstructions of the Austre Lovénbreen glacier based on aerial imagery from 1923 (Mittelholzer, 1923) and 1936 (Girod et al., 2018) show the glacier elevation up to 75 m (55 m at Profile A-A'; Fig. 7A) above the current level. These reconstructions potentially depict the state of the Austre Lovénbreen close to the maximum extent in the Holocene, as the Little Ice Age (LIA) ended on Svalbard in the 1920s (Svendsen and Mangerud, 1997) and that the LIA corresponds well with the maximum glacier extent of the Holocene (Snyder et al., 2000; Humlum et al., 2005; Błaszczyk et al., 2009; Martín-Moreno and Allende-Álvarez, 2016; Farnsworth et al., 2020). Therefore, a glacial origin of the subsurface ice layer up to 75 m above the current glacier level can be assumed.

Indicating that the dead ice within the lower sections of the slopes (max. glacier elevation) is at least 85 years old and potentially much older in the upper section. As Bernard et al. (2024) has shown for the lower sections that the ice within the slopes (e.g. Section II, Fig. 5) is still present decades after the glacier has retreated from the foot of the slope. In contrast the conceptual model of morphological slope evolution based on vegetation studies at Colletthøgda assumed that the melting of the last dead-ice bodies (10–150 m a.s.l.) occurs after roughly 35 years (Mercier et al., 2009) or 50–60 years in ice-cored moraines in Svalbard (Ewertowski and Tomczyk, 2020) after deglaciation.

Formation of segregation ice within the debris could be responsible for the ice within the upper slopes of the Austre Lovénbreen basin. However, a glacial origin cannot be entirely discarded, considering the

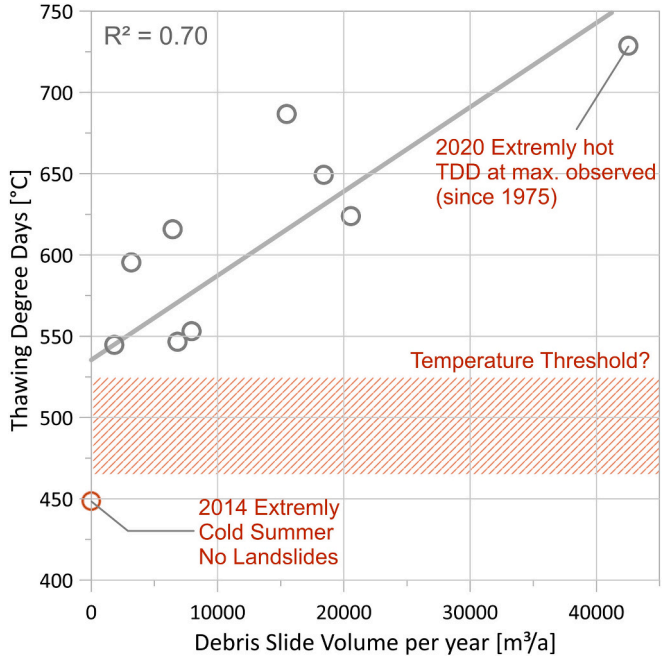

Fig. 14. The thermal dependency of debris slide formation with the Austre Lovénbreen basin. No debris slides were observed within a year when the TDD was below 545 °C.

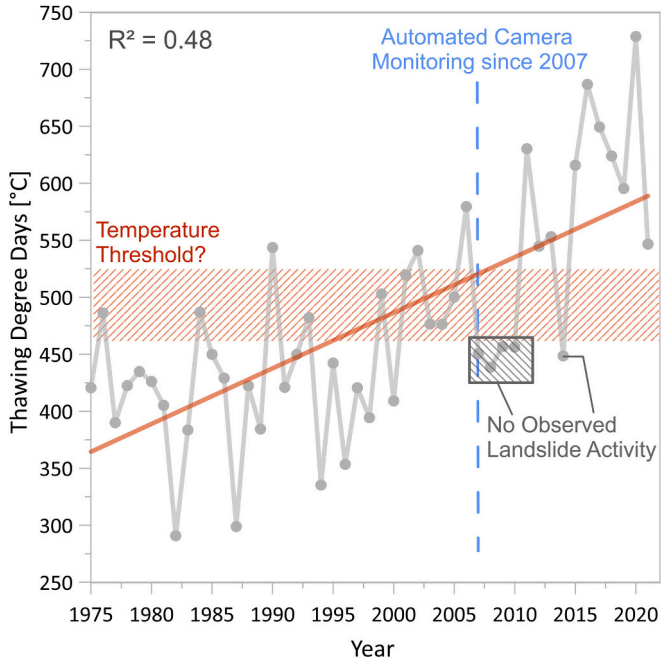

Fig. 15. Increase of TDD in Ny-Ålesund since 1975. Since implementing the automated camera network, only five years were observed without debris slide activity (TDD below 545 °C), indicating a temperature threshold for debris slide activity.

thickness and continuity of the observed ice layer up to 245 m a.s.l. at the current glacier terminus (~130 m a.s.l.) (Fig. 4). Thus, ice sampling and age dating are required to assess the origin of the ice layer and the spatial extent within Section 1 (Fig. 5).

Furthermore, the visual resemblance of smaller debris slide deposits to pro-talus ramparts and larger ones to ice-cored rock glaciers prompts the question of whether these landforms could potentially evolve into

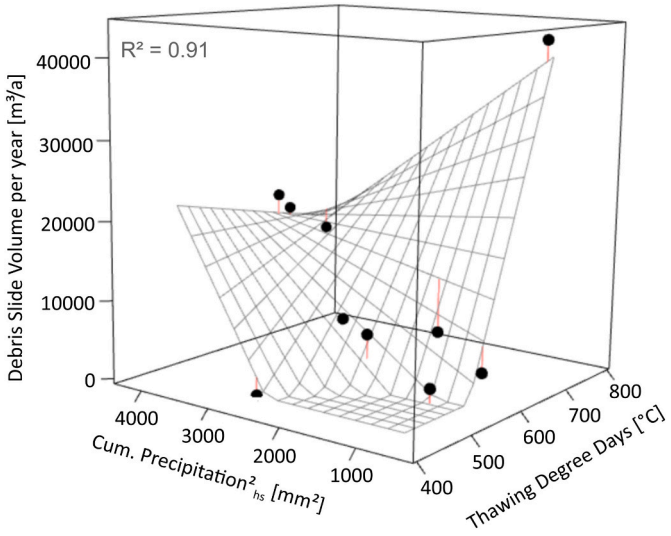

Fig. 16. Impact of temperature and (TDD) and precipitation (Cum. Precipitation^{2}hs) on the debris slide formation per year (R^2 = 0.91). Residuals are indicated in red.

talus-derived rock glaciers over time, provided suitable conditions. However, as global warming is projected to increase rainfall amounts, facilitate the thickening of the active layer, and thus increase erosion rates in the Arctic (Christiansen et al., 2010; Førland et al., 2011; De Haas et al., 2015; Bernhardt et al., 2017; Lønne, 2017) it is possible that the ice within slopes and the debris slide deposits will decay in the next decades.

5.3. Spatiotemporal variation of dominant process types within the paraglacial period

The spatial occurrence and extent of the subsurface ice layer within the slopes was identified as the main predisposition factor determining the dominant process type, as shown by the shift from debris slides towards debris flows (Fig. 5; Sections 1 and 3). Mercier et al. (2009) described a similar lateral succession of different processes at *Colletthøgda* (7.5 km north-east from the study site), with translational slides in proximity to the glacier that are succeeded by debris flows, gullying and rill erosion during later stages of paraglacial slope evolution.

Debris flows are generally considered the primary source of erosion and sediment transport acting within the paraglacial period (Owen, 1991; Ballantyne and Benn, 1994; Evans and Clague, 1994; Curry, 1999; Ballantyne, 2002; Chiarle et al., 2007; Ewertowski and Tomczyk, 2020). However, modification of steep sediment-mantled slopes by translational debris slides may be extensive given recent glacier retreat (Ballantyne, 2002) and thus is limited by a temporal and spatial component. Similar observations were made on ice-cored scree slopes and moraines in Svalbard (Mercier et al., 2009; Lønne, 2017; Ewertowski and Tomczyk, 2020), the Canadian Rocky Mountains (Mattson and Gardner, 1991), and the Vestfold hills in East Antarctica (Fitzsimons, 1996).

The paraglacial sediment transport pre-dominantly by translational debris slides within the Austre Lovénbreen basin indicates that the slope system is generally at an early stage of development. Observed debris flows, and associated landforms (e.g., levees and debris cones) only dominate the oldest slope sections (Fig. 5, Section I). The impact of debris flows was marginal for the entire basin (3.9 %; 4982 m^3 ± 886 m^3) and was primarily located in Section I (2,9 %; 3710 ± 645 m^3). Thus, Section I may present a more advanced and to a degree stable stage of slope development. The initial strong sediment flux by translational debris slides is followed by a decline of available unstable

sediment sources until only sporadic debris flow activity remains. Our observation fits well into the concept of an exponential exhaustion model of paraglacial sediment reworking.

However, the importance of translational debris slides on paraglacial slope modification may also be underestimated, given a lack of data with a high spatiotemporal resolution. Debris slides and associated landforms (e.g. scarps, deposits) are overprinted or eroded by other processes as seen in several studies (Lønne and Lysså, 2005; Mercier et al., 2009; Lønne, 2017). While other studies (Eckerstorfer et al., 2013; De Haas et al., 2015; Tomczyk, 2021) suggest that snow avalanches are a dominant slope-forming process, their erosional capabilities in this study were found to be marginal. Even after a 10-year observation period, no entrainment channels or other significant surface changes (below LOD95%) caused by snow avalanches were detected, except for the erosion of small-scale features, such as debris slide scars, notably at Profile A-A' (Fig. 7). The absence of translational debris slides or older debris slide deposits within Section I may be attributed to overprinting by debris flows and snow avalanches. Thus, it remains uncertain to which degree snow avalanches affect the evolution of sediment-mantled slopes in Svalbard.(Lønne, 2017).

5.4. Impact of meteorological factors

Meteorological factors exert a significant influence on landslide dynamics (Crozier, 2010; Gariano and Guzzetti, 2016; Patton et al., 2019) and are therefore directly linked to climatic conditions (Soldati et al., 2004; Gariano and Guzzetti, 2016; Matthews et al., 2018; Patton et al., 2019). Our analysis demonstrates that meteorological factors predominantly account for both the frequency and magnitude of debris slides observed over a 10-year period (Fig. 16) within a high-arctic glacier basin. Consequently, these factors are responsible for driving the majority (96 %) of paraglacial sediment transport. In contrast, previous case studies in other comparable paraglacial environments, such as the Fåbergstølsdalen (Ballantyne and Benn, 1994) and Colletthøgda (Mercier et al., 2009) found that paraglacial sediment transfer by debris flows or debris slides occurs annually on steep sediment-mantled slopes and is not dependent on meteorological extreme events. However, the comparability of those case studies may be limited as the annual average rainfall found at the Fåbergstølsdalen (Central Norway) is considerably higher than at Kongsfjorden. Thus, it is more likely that rainfall thresholds necessary for debris flow initiation could have been reached every year at the Fåbergstølsdalen. The observation period at Colletthøgda was limited because fieldwork was only conducted in 1996 and 2004.

5.5. Debris slides initiation and trigger mechanisms

Heavy rainfall events during the hydrological summer are the main triggering factor contributing to the magnitude and frequency of debris slides (Fig. 13). Snow melt and heavy rainfall events during the early summer did not cause debris slides, as the percolation of rainwater within a frozen debris body towards the ice-debris interface may be limited. The duration and intensity of the thawing period (expressed by TDD) and thus the maximum annual thaw depth (ATD) during a given calendar year was identified as the primary control for debris slide formation (Figs. 14 & 15).

Similarly, Mattson and Gardner (1991) found that heavy rainfall and temperature increases contributed to rapid translational debris slides along ice layers near the Boundary Glacier, Alberta. They linked warm weather to five such slides (N = 25), though these were smaller, contributing just 14 % of the total sediment flux. At Austre Lovénbreen, only nine temperature-induced slides (N = 107) were identified, but these had above-average magnitudes (1132 ± 150 m^3) (Fig. 12, indicated in red). Additionally, Mercier et al. (2009) described extensive erosion rates primarily caused by meltwater-induced translational slides and dead ice scouring in areas adjacent to the glacier margin. Other studies in Svalbard (e.g. Lønne, 2017; Ewertowski and Tomczyk, 2020) have also indicated that either the base of the active layer or buried glacier ice may be the main rupture surface for small landslides on ice-cored moraines.

Our observations support the hypothesis, that the thaw horizon has to reach the ice layer in order to trigger debris slides and thus a certain temperature threshold is needed (Fig. 15). This is consistent with the fact that no debris slides were recorded below an annual temperature threshold (TDD ~545 °C) and the strong correlation between the TDD and debris slide activity during a year ($R = 0.70$). Furthermore, a cluster of debris slide events without any rainfall occurred in 2020, when the warmest summer period was registered (TDD >700 °C), indicating that increased ablation of the subsurface ice layer may cause debris slides independent from rainfall event as also found at the Boundary Glacier (Mattson and Gardner, 1991) (Fig. 12).

Although the dataset is too limited to define a precise temperature threshold for debris slide activity within the Austre Lovénbreen basin, a temperature range between years of debris slide activity (minimum TDD ~545 °C) and inactivity (TDD ~450 °C) can be identified (Figs. 14 & 15). Notably, the ongoing downwastage of the glacier at the slope base did not directly cause translational debris slides but led to slope adjustments through creep processes, as observed in years with a TDD below 545 °C (2007 to 2011, and 2014).

Correlation between individual debris slides initiation and TDD was investigated, as the depth of thaw is positively correlated with TDD, using a simplified variant of the Stefan equation:

$$Z = E\sqrt{TDD} \quad (1)$$

where Z is the depth of thaw; TDD the Thawing Degree Days (TDD); and E is the edaphic factor, a site-specific scaling parameter (Stefan, 1890; Hinkel and Nicholas, 1995; Strand et al., 2021). Site-specific E-values for the Austre Lovénbreen basin were calculated using either the maximum TDD within a year or the TDD at the time of debris slide initiation (TDD @ failure). Thaw depth was assumed to be the thickness of the dated debris slides, as the rupture surface was consistently the subsurface ice layer. However, E-values varied significantly, with no correlation to debris cover thickness. This variation may be due to snow cover differences, rainfall impacts on non-conductive heat transfer, and varying trigger mechanisms (e.g. rainfall or temperature induced) given the relative homogenous material found on the slopes. A 3D modelling approach and expanded monitoring would be needed to assess spatial variations.

A weak correlation (R = 0.26) was observed between Freezing Degree Days (FDD) and annual debris slide activity. While FDD is employed to quantify the thermal reset between two thaw periods, it is not an entirely reliable metric for this purpose. As the impact of FDD on ATD also depends on the thickness, duration, and consistency of the snow cover (Strand et al., 2021). Therefore, climate change can be expected to further facilitate the observed debris slide activity, given that temperature thresholds during the thawing or freezing period will be exceeded in the future.

5.5.1. Debris slides initiation and trigger mechanisms

Major debris flows (≥400 m^3; N = 5) required over 25 mm of rainfall to occur, as revealed by data from the automated camera network. The largest debris flows (~1000 m^3; N = 2) were triggered by rainfall events of 39.70 mm per day in 2016 and 37 mm per day in 2021. Smaller debris flows (≤200 m^3) were not detected, likely due to insufficient camera resolution or their occurrence in areas beyond the camera's coverage. Debris flows were also not observed in years below a TDD of ~545 °C, which may be due to the smaller sample size or due to the above-explored data biases affecting small-scale events.

Debris flows were detected in only 4 out of the 10 years of available TLS data (Fig. 8), exhibiting non-linear temporal variations characterised by aperiodic fluctuations, rather than demonstrating a linear

trend or correlation annual averages (e.g. Birks, 1991; Miller et al., 2010; Turner and Marshall, 2011; Bernhardt et al., 2017). Statistical correlation with individual heavy rainfall events was limited due to the limited observations (Table 1). Debris flows initiation by snowmelt, as found by other studies conducted in the arctic (Jahn, 1976; Strömquist, 1976; Larsson, 1982; André, 1990a; André, 1990b; Bernhardt et al., 2017), could not be observed. Debris flows initiated by debris slides (debris flowslide after the Varnes classification; Hungr et al. (2014)), as seen by Ballantyne and Benn (1994) at the Fåbergstølsbreen (Norway), could also not be observed within the study area. Most likely, as debris flowslides require excess pore-pressure or liquefaction of material originating from the landslide source (Hungr et al., 2014). The lack of rainfall in the Kongsfjorden area compared to Fåbergstølsbreen and a well-drained sediment-body, as found on the slopes of the Austre Lovénbreen basin, may impede their development.

Previous studies found recurrence periods for major debris flows ($\geq$400 m^3) at Hanaskogdalen (Svalbard) to range between 5 and 10 years between 1961 and 2013 (Bernhardt et al., 2017), which is up to two orders of magnitude shorter than older estimations for Svalbard or northern Scandinavia (80 to 500 years) (Strömquist, 1976; Rapp and Nyberg, 1981; André, 1986; André, 1990b). Between 2011 and 2021, our observations show that major debris flows in Austre Lovénbreen occur with a 2-year recurrence period, which is an increase by a factor of 2.5 to 5 when compared to Hanaskogdalen. Additionally, we identified a 5-year recurrence period for even larger debris flows ($\sim$1000 m^3). However, similar average debris flow volumes in both regions (Hanaskogdalen: $\sim$220 m^3; Austre Lovénbreen basin: $\sim$237 $\pm$ 42 m^3) and comparable annual net deposition rates (Hanaskogdalen: $\sim$480 m^3; Austre Lovénbreen basin: $\sim$498 $\pm$ 89 m^3) could be found (Bernhardt et al., 2017).

Based on our analysis, several factors likely contribute to the differences in debris flow magnitude observed between the two case studies. Firstly, the average annual precipitation at Ny-Ålesund is notably higher than at Svalbard Airport (Førland et al., 2011), which results in more frequent and intense rainfall events conducive to debris flow initiation. Secondly, debris flow initiation in Hanaskogdalen may be facilitated by its significantly larger catchment area, allowing water to accumulate over a larger area and thereby increasing the total water available for runoff in the channel. Moreover, the increase in heavy rainfall events at Ny-Ålesund caused by climate change as the annual precipitation increased about 3–5 % per decade (Førland et al., 2011; Maturilli et al., 2019) (Fig. 2). Lastly, differences in sediment availability, influenced by the different lithologies, may affect the propensity for debris flow occurrence.

Nevertheless, due to the susceptibility of short data sets to extrapolation errors, neither the frequency or magnitude of debris flows, nor the net deposition rates, can be considered reliable climate change proxies. Further investigation into these factors is imperative for a thorough understanding of long-term debris flow dynamics in Arctic environments.

6. Conclusions

Landslide processes affecting steep sediment-mantled slopes in the studied Austre Lovénbreen basin are investigated based on several methods, consisting of (i) geomorphological mapping, (ii) multi-temporal TLS surveys, and (iii) visual monitoring via an automated camera network and subsequent image analysis.

Multi-temporal TLS campaigns with a high spatial resolution allowed us to detect and quantify complex terrain changes between the TLS campaigns within the level of detection in the range of centimetres (LOD95%). The combined analysis of quantitative TLS data with qualitative data from the automated camera network allowed for investigating the impact of meteorological factors on debris slide trigger mechanisms, kinematics and the evolution of paraglacial slopes following glacier retreat and downwastage.

Landslide phenomena were the most dominant source of surface change, with respect to the retreat of the glacier itself, during the observation period. Debris slides accounted for 96 % of paraglacial sediment transport affecting sediment-mantled slopes in the studied Austre Lovénbreen basin and are controlled by a combination of meteorological factors, foremost rainfall and temperature. The spatial distribution of an ice-layer within slopes serving as the rupture surface of observed translational debris slides and the thermal regime during a year are the main aspects enabling potential translational debris slides. However, heavy rainfall events within the hydrological summer are the main factor contributing to the magnitude and frequency of the debris slides. A weak correlation between debris flow activity and increased rainfalls during the observation period could be found.

Furthermore, there is a noticeable transition from debris slides to debris flows corresponding to stages of the ongoing glacier retreat, indicating a lateral succession of geomorphological processes that dominate the paraglacial evolution. Specifically, debris slide frequency and magnitude decreased with distance to the glacier, while the occurrence of debris flows increased.

Finally, the increased debris slide frequency and magnitude within the observation period showed the acceleration of climate-induced changes modifying the landscape within this high-Arctic environment. Our results show that the intensity of the thawing period and heavy rainfall events are crucial for paraglacial adjustment of steep sediment-mantled slopes through debris slides. The recurrence periods of large debris flows ($\geq$400 m^3) have decreased by a factor of at least 2.5 to 5 compared to findings from other studies conducted in the past decade on Svalbard. The expected continuous temperature rise and heavy rainfall events may further facilitate landslide processes in the Arctic.

We stress that long-term observatories, such as the Austre Lovénbreen glacier basin, are irreplaceable for future research focusing on glacial and paraglacial responses to climate change in the high-Arctic as the quantification of these processes may serve as additional climate change proxies to indicate past and present climate alterations and may provide insights also relevant for other regions as climate change is more pronounced at higher latitudes.

CRediT authorship contribution statement

Erik Kuschel: Writing – original draft, Visualization, Methodology, Investigation, Formal analysis, Data curation, Conceptualization. **Florian Tolle:** Writing – review & editing, Project administration, Investigation, Funding acquisition, Conceptualization. **Vinzent Klaus:** Writing – review & editing, Formal analysis. **Ursula Laa:** Visualization, Formal analysis. **Alexander Prokop:** Investigation, Data curation. **Jean-Michel Friedt:** Software, Investigation, Data curation. **Eric Bernard:** Investigation. **Christian Zangerl:** Writing – review & editing, Supervision, Investigation.

Declaration of competing interest

The authors declare that they have no known competing financial interests or personal relationships that could have appeared to influence the work reported in this paper.

Acknowledgements

This study is part of the PRISM project, supported by the French Polar Institute Paul-Émile Victor (IPEV), French Agence Nationale de la Recherche, Région Bourgogne Franche-Comté, and CNRS Groupement de Recherche Arctique. Open access funding is provided by BOKU University, Austria. We would like to express our sincere gratitude to Christopher Lüthgens for his invaluable contributions to the geomorphological discussion, and to Stephanie Neuhuber for her expert editing and redaction. Your insights and efforts have greatly enhanced our work. Furthermore, we want to acknowledge the two anonymous

reviewers for their input.

Data availability

Data will be made available on request.

References

Abellán, A., Oppikofer, T., Jaboyedoff, M., Rosser, N.J., Lim, M., Lato, M.J., 2014. Terrestrial laser scanning of rock slope instabilities. Earth Surf. Process. Landf. 39. https://doi.org/10.1002/esp.3493.

Agliardi, F., Crosta, G., Zanchi, A., 2001. Structural constraints on deep-seated slope deformation kinematics. Eng. Geol. 59. https://doi.org/10.1016/S0013-7952(00)00066-1.

André, M., 1986. Dating slope deposits and estimating rates of rock wall retreat in northwest Spitsbergen by lichenometry. Geografiska Annaler, Series A 68 A. https://doi.org/10.1080/04353676.1986.11880159.

André, 1990a. Geomorphic impact of spring avalanches in Northwest Spitsbergen (79° N). Permafr. Periglac. Process. 1. https://doi.org/10.1002/ppp.3430010203.

André, 1990b. Frequency of debris flows and slush avalanches in Spitsbergen: a tentative evaluation from lichenometry. Pol. Polar. Res. 11.

Ballantyne, C.K., 2002. Paraglacial geomorphology. Quat. Sci. Rev. 21 (18–19), 1935–2017.

Ballantyne, C.K., Benn, D.I., 1994. Paraglacial slope adjustment and resedimentation following recent glacier retreat, Fabergstolsdalen, Norway. Arct. Alp. Res. 26. https://doi.org/10.2307/1551938.

Barbaroux, L., 1967. Le Quaternaire de la Péninsule de Broker et régions voisines (Spitsberg occidental). Bulletin de l'Association française pour l'étude du quaternaire 4. https://doi.org/10.3406/quate.1967.1068.

Bergh, S.G., Maher, H.D., Braathen, A., 2000. Tertiary divergent thrust directions from partitioned transpression, Broggerhalvoya, Spitsbergen. Norsk Geologisk Tidsskrift 80. https://doi.org/10.1080/002919600750042573.

Bernard, É., Friedt, J.M., Tolle, F., Griselin, M., Martin, G., Laffly, D., Marlin, C., 2013. Monitoring seasonal snow dynamics using ground based high resolution photography (Austre Lovénbreen, Svalbard, 79°N). ISPRS J. Photogramm. Remote. Sens. 75. https://doi.org/10.1016/j.isprsjprs.2012.11.001.

Bernard, É., Friedt, J.M., Saintenoy, A., Tolle, F., Griselin, M., Marlin, C., 2014. Where does a glacier end? GPR measurements to identify the limits between valley slopes and actual glacier body. Application to the Austre Lovénbreen, Spitsbergen. Int. J. Appl. Earth Obs. Geoinf. 27. https://doi.org/10.1016/j.jag.2013.07.006.

Bernard, E., Friedt, J.M., Prokop, A., Tolle, F., Griselin, M., 2024. Is a glacier gone when it looks gone? Subsurface characteristics of high-Arctic ice-cored slopes as evidence of the latest maximum glacier extent. Earth Surf Process Landf. https://doi.org/10.1002/esp.5894.

Bernhardt, H., Reiss, D., Hiesinger, H., Hauber, E., Johnsson, A., 2017. Debris flow recurrence periods and multi-temporal observations of colluvial fan evolution in central Spitsbergen (Svalbard). Geomorphology 296. https://doi.org/10.1016/j.geomorph.2017.08.049.

Besl, P.J., McKay, N.D., 1992. A method for registration of 3-D shapes. IEEE Trans. Pattern Anal. Mach. Intell. 14. https://doi.org/10.1109/34.121791.

Birks, H.H., 1991. Holocene vegetational history and climatic change in west Spitsbergen - plant macrofossils from Skardtjørna, an Arctic lake. Holocene 1. https://doi.org/10.1177/095968369100100303.

Błaszczyk, M., Jania, J.A., Hagen, J.O., 2009. Tidewater glaciers of Svalbard: recent changes and estimates of calving fluxes. Pol. Polar Res. 30.

Bowden, W.B., Gooseff, M.N., Balser, A., Green, A., Peterson, B.J., Bradford, J., 2008. Sediment and nutrient delivery from thermokarst features in the foothills of the North Slope, Alaska: potential impacts on headwater stream ecosystems. Eur. J. Vasc. Endovasc. Surg. 113. https://doi.org/10.1029/2007JG000470.

Chen, Y., Medioni, G., 1991. Object modeling by registration of multiple range images. In: Proceedings - IEEE International Conference on Robotics and Automation. https://doi.org/10.1109/robot.1991.132043.

Chiarle, M., Iannotti, S., Mortara, G., Deline, P., 2007. Recent debris flow occurrences associated with glaciers in the Alps. Glob. Planet Chang. 56. https://doi.org/10.1016/j.gloplacha.2006.07.003.

Christiansen, H.H., Etzelmüller, B., Isaksen, K., Juliussen, H., Farbrot, H., Humlum, O., Johansson, M., Ingeman-Nielsen, T., Kristensen, L., Hjort, J., Holmlund, P., Sannel, A.B.K., Sigsgaard, C., Åkerman, H.J., Foged, N., Blikra, L.H., Pernosky, M.A., Ødegård, R.S., 2010. The thermal state of permafrost in the nordic area during the international polar year 2007-2009. Permafr. Periglac. Process. 21. https://doi.org/10.1002/ppp.687.

Christiansen, H., Humlum, O., Eckerstorfer, M., 2013. Central svalbard 2000-2011 meteorological dynamics and periglacial landscape response. Arct. Antarct. Alp. Res. 45. https://doi.org/10.1657/1938-4246-45.16.

Church, M., Ryder, J.M., 1972. Paraglacial sedimentation: a consideration of fluvial processes conditioned by glaciation. Bull. Geol. Soc. Am. 83. https://doi.org/10.1130/0016-7606(1972)83[3059:PSACOF]2.0.CO;2.

CloudCompare, 2021. CloudCompare Version 2.13.

Crozier, M.J., 2010. Deciphering the effect of climate change on landslide activity: a review. Geomorphology. https://doi.org/10.1016/j.geomorph.2010.04.009.

Cruden, D.M., 1991. A simple definition of a landslide. Bull. Int. Assoc. Eng. Geol. Bulletin de l'Association Internationale de Géologie de l'Ingénieur 43. https://doi.org/10.1007/BF02590167.

Cruden, D.M., Varnes, D.J., 1996. Landslide Types and Processes. Special Report - National Research Council, Transportation Research Board, p. 247.

Curry, A.M., 1999. Paraglacial modification of slope form. Earth Surf. Process. Landf. 24. https://doi.org/10.1002/(SICI)1096-9837(199912)24:13<1213::AID-ESP32>3.0.CO;2-B.

De Haas, T., Kleinhans, M.G., Carbonneau, P.E., Rubensdotter, L., Hauber, E., 2015. Surface morphology of fans in the high-Arctic periglacial environment of Svalbard: controls and processes. Earth Sci. Rev. 146, 163–182. https://doi.org/10.1016/J.EARSCIREV.2015.04.004.

Eckerstorfer, M., Christiansen, H., 2011. The "high arctic maritime snow climate" in Central svalbard. Arct. Antarct. Alp. Res. 43. https://doi.org/10.1657/1938-4246-43.1.11.

Eckerstorfer, M., Christiansen, H.H., Vogel, S., Rubensdotter, L., 2013. Snow cornice dynamics as a control on plateau edge erosion in central Svalbard. Earth Surf. Process. Landf. 38. https://doi.org/10.1002/esp.3292.

Evans, S.G., Clague, J.J., 1994. Recent climatic change and catastrophic geomorphic processes in mountain environments. Geomorphology 10. https://doi.org/10.1016/0169-555X(94)90011-6.

Ewertowski, M.W., Tomczyk, A.M., 2020. Reactivation of temporarily stabilized ice-cored moraines in front of polythermal glaciers: Gravitational mass movements as the most important geomorphological agents for the redistribution of sediments (a case study from Ebbabreen and Ragnarbreen, Svalbard). Geomorphology 350. https://doi.org/10.1016/j.geomorph.2019.106952.

Fahnestock, M.A., Scambos, T.A., Bindschadler, R.A., 1992. Semi-automated ice velocity determination from satellite imagery. Eos (Washington DC) 73.

Farnsworth, W.R., Allaart, L., Ingólfsson, Ó., Alexanderson, H., Forwick, M., Noormets, R., Retelle, M., Schomacker, A., 2020. Holocene glacial history of Svalbard: status, perspectives and challenges. Earth Sci Rev. https://doi.org/10.1016/j.earscirev.2020.103249.

Fey, C., Wichmann, V., 2017. Long-range terrestrial laser scanning for geomorphological change detection in alpine terrain – handling uncertainties. Earth Surf. Process. Landf. 42. https://doi.org/10.1002/esp.4022.

Fitzsimons, S.J., 1996. Paraglacial redistribution of glacial sediments in the Vestfold Hills, East Antarctica. Geomorphology 15. https://doi.org/10.1016/0169-555X(95)00122-L.

Førland, E.J., Benestad, R., Hanssen-Bauer, I., Haugen, J.E., Skaugen, T.E., 2011. Temperature and precipitation development at Svalbard 1900–2100. Adv. Meteorol. 2011. https://doi.org/10.1155/2011/893790.

Francis, J.A., Vavrus, S.J., Cohen, J., 2017. Amplified Arctic warming and mid-latitude weather: new perspectives on emerging connections. Wiley Interdiscip. Rev. Clim. Chang. 8. https://doi.org/10.1002/wcc.474.

French, H.M., 2013. The Periglacial Environment: Third edition, The Periglacial Environment: Third Edition. https://doi.org/10.1002/9781118684931.

Friedt, J.M., Tolle, F., Bernard, É., Griselin, M., Laffly, D., Marlin, C., 2012. Assessing the Relevance of Digital Elevation Models to Evaluate Glacier Mass Balance: Application to Austre Lovénbreen (Spitsbergen, 79°N), in: Polar Record. https://doi.org/10.1017/S0032247411000465.

Friedt, J.M., Bernard, É., Griselin, M., 2023. Ground-based oblique-view photogrammetry and sentinel-1 spaceborne RADAR reflectivity snow melt processes assessment on an arctic glacier. Remote Sens. (Basel) 15. https://doi.org/10.3390/rs15071858.

Gariano, S.L., Guzzetti, F., 2016. Landslides in a changing climate. Earth Sci. Rev. https://doi.org/10.1016/j.earscirev.2016.08.011.

Girod, L., Ivar Nielsen, N., Couderette, F., Nuth, C., Kääb, A., 2018. Precise DEM extraction from Svalbard using 1936 high oblique imagery. Geosci. Instrum. Methods Data Syst. 7. https://doi.org/10.5194/gi-7-277-2018.

Hagen, J.O., Kohler, J., Melvold, K., Winther, J.G., 2003. Glaciers in Svalbard: mass balance, runoff and freshwater flux. Polar Res. 22. https://doi.org/10.1111/j.1751-8369.2003.tb00104.x.

Hinkel, K.M., Nicholas, J.R., 1995. Active layer thaw rate at a boreal forest site in central Alaska, USA. Arct. Alp. Res. 27. https://doi.org/10.2307/1552069.

Hjelle, A.Q.Y., Piepjohn, K., Saalmann, K., Salvigsen, O., Thiedig, F., Dallmann, K., 1999. Geological map of Svalbard 1:100 000, sheet A7G Kongsfjorden. Norsk Polarinstitutt Temakart no. 22, 56 pp.

Hong, E., Perkins, R., Trainor, S., 2014. Thaw settlement hazard of permafrost related to climate warming in Alaska. Arctic 67. https://doi.org/10.14430/arctic4368.

Huggel, C., Clague, J.J., Korup, O., 2012. Is climate change responsible for changing landslide activity in high mountains? Earth Surf. Process. Landf. 37. https://doi.org/10.1002/esp.2223.

Humlum, O., Elberling, B., Hormes, A., Fjordheim, K., Hansen, O.H., Heinemeier, J., 2005. Late-Holocene glacier growth in Svalbard, documented by subglacial relict vegetation and living soil microbes. Holocene 15. https://doi.org/10.1191/0959683605hl817rp.

Hungr, O., Leroueil, S., Picarelli, L., 2014. The Varnes classification of landslide types, an update. Landslides. https://doi.org/10.1007/s10346-013-0436-y.

IPCC, 2014. Climate Change 2014: Synthesis Report. Contribution of Working Groups I, II and III to the Fifth Assessment Report of the Intergovernmental Panel on Climate Change, Ipcc.

IPCC, 2021. Climate Change 2021: The Physical Science Basis. Working Group I Contribution to the IPCC Sixth Assessment Report. Climate Change 2021: The Physical Science Basis.

Irvine-Fynn, T.D.L., Hodson, A.J., Moorman, B.J., Vatne, G., Hubbard, A.L., 2011. Polythermal glacier hydrology: a review. Rev. Geophys. https://doi.org/10.1029/2010RG000350.

Jahn, A., 1976. Contemporaneous geomorphological processes in Longyeardalen, Vestspitsbergen (Svalbard). Biul. Peryglac. 26.

Lague, D., Brodu, N., Leroux, J., 2013. Accurate 3D comparison of complex topography with terrestrial laser scanner: application to the Rangitikei canyon (N-Z). ISPRS J. Photogramm. Remote Sens. 82. https://doi.org/10.1016/j.isprsjprs.2013.04.009.
Larsson, S., 1982. Geomorphological effects on the slopes of Longyear Valley, Spitsbergen, after a heavy rainstorm in July 1972. Geografiska Annaler, Series A 64 A. https://doi.org/10.1080/04353676.1982.11880059.
Leibman, M.O., 1995. Cryogenic landslides on the Yamal Peninsula, Russia: preliminary observations. Permafr. Periglac. Process 6. https://doi.org/10.1002/ppp.3430060307.
Leibman, M., Khomutov, A., Kizyakov, A., 2014. Cryogenic landslides in the West-Siberian plain of Russia: classification, mechanisms, and landforms. Environ. Sci. Eng. https://doi.org/10.1007/978-3-319-00867-7_11.
Lewkowicz, A.G., Harris, C., 2005. Frequency and magnitude of active-layer detachment failures in discontinuous and continuous permafrost, northern Canada. Permafr. Periglac. Process 16. https://doi.org/10.1002/ppp.522.
Lønne, I., 2017. Terrestrial slopes in northern high latitudes: a paradigm shift regarding sediment origin, composition, and dynamic evolution. Geomorphology 276. https://doi.org/10.1016/j.geomorph.2016.10.004.
Lønne, I., Lyså, A., 2005. Deglaciation dynamics following the Little Ice Age on Svalbard: Implications for shaping of landscapes at high latitudes. Geomorphology 72. https://doi.org/10.1016/j.geomorph.2005.06.003.
Macfarlane, D.F., 2009. Observations and predictions of the behaviour of large, slow-moving landslides in schist, Clyde Dam reservoir, New Zealand. Eng. Geol. 109. https://doi.org/10.1016/j.enggeo.2009.02.005.
Marlin, C., Tolle, F., Griselin, M., Bernard, E., Saintenoy, A., Quenet, M., Friedt, J.M., 2017. Change in geometry of a high arctic glacier from 1948 to 2013 (Austre Lovénbreen, Svalbard). Geogr. Ann. Ser. B 99. https://doi.org/10.1080/04353676.2017.1285203.
Martín-Moreno, R., Allende-Álvarez, F., 2016. Little Ice Age glacier extension and retreat in Spitsbergen Island (High Arctic, Svalbard Archipelago). Cuadernos de Investigación Geográfica 42. https://doi.org/10.18172/cig.2919.
Masson-Delmotte, V., Kageyama, M., Braconnot, P., Charbit, S., Krinner, G., Ritz, C., Guilyardi, E., Jouzel, J., Abe-Ouchi, A., Crucifix, M., Gladstone, R.M., Hewitt, C.D., Kitoh, A., LeGrande, A.N., Marti, O., Merkel, U., Motoi, T., Ohgaito, R., Otto-Bliesner, B., Peltier, W.R., Ross, I., Valdes, P.J., Vettoretti, G., Weber, S.L., Wolk, F., Yu, Y., 2006. Past and future polar amplification of climate change: climate model intercomparisons and ice-core constraints. Climate Dynam. 26. https://doi.org/10.1007/s00382-005-0081-9.
Matthews, J.A., Winkler, S., Wilson, P., Tomkins, M.D., Dortch, J.M., Mourne, R.W., Hill, J.L., Owen, G., Vater, A.E., 2018. Small rock-slope failures conditioned by Holocene permafrost degradation: a new approach and conceptual model based on Schmidt-hammer exposure-age dating, Jotunheimen, southern Norway. Boreas 47. https://doi.org/10.1111/bor.12336.
Mattson, L.E., Gardner, J.S., 1991. Mass wasting on valley-side ice-cored moraines, Boundary Glacier, Alberta, Canada. Geografiska Annaler, Series A 73 A. https://doi.org/10.1080/04353676.1991.11880337.
Maturilli, M., Hanssen-Bauer, I., Neuber, R., Rex, M., Edvardsen, K., 2019. The Atmosphere Above Ny-Ålesund: Climate and Global Warming, Ozone and Surface UV Radiation. https://doi.org/10.1007/978-3-319-46425-1_2.
Mercier, D., Étienne, S., Sellier, D., André, M.F., 2009. Paraglacial gullying of sediment-mantled slopes: a case study of Colletthøgda, Kongsfjorden area, West Spitsbergen (Svalbard). Earth Surf. Process. Landf. 34, 1772–1789. https://doi.org/10.1002/esp.1862.
MET Norway, 2024. Norwegian Meteorological Institut.
Miller, G.H., Brigham-Grette, J., Alley, R.B., Anderson, L., Bauch, H.A., Douglas, M.S.V., Edwards, M.E., Elias, S.A., Finney, B.P., Fitzpatrick, J.J., Funder, S.V., Herbert, T.D., Hinzman, L.D., Kaufman, D.S., MacDonald, G.M., Polyak, L., Robock, A., Serreze, M. C., Smol, J.P., Spielhagen, R., White, J.W.C., Wolfe, A.P., Wolff, E.W., 2010. Temperature and precipitation history of the Arctic. Quat. Sci. Rev. 29. https://doi.org/10.1016/j.quascirev.2010.03.001.
Mittelholzer, W., 1923. Kingsbai mit Kingsgletscher und Lovenfirnen von Osten aus 1700 m Höhe-Spitzbergenflug 1923. ETH-Bibliothek_LBS_MH02-01-0041. https://commons.wikimedia.org/wiki/Category:ETH-BIB_Mittelholzer-Spitsbergen_flight_1923.
Nordli, Ø., Przybylak, R., Ogilvie, A.E.J., Isaksen, K., 2014. Long-term temperature trends and variability on spitsbergen: the extended svalbard airport temperature series, 1898-2012. Polar Res. 33. https://doi.org/10.3402/polar.v33.21349.
NPI, 2014. Terrengmodell Svalbard (S0 Terrengmodell) [Data set]. Norwegian Polar Institute. https://doi.org/10.21334/npolar.2014.dce53a47.
Owen, L.A., 1991. Mass Movement Deposits in the Karakoram Mountains: Their Sedimentary Characteristics, Recognition and Role in Karakoram Landform Evolution.
Panholzer, H., Prokop, A., 2013. Wedge-filtering of geomorphologic terrestrial laser scan data. Sensors (Switzerland) 13. https://doi.org/10.3390/s130202579.
Panholzer, H., Prokop, A., 2018. HOVE-Wedge-filtering of geomorphologic terrestrial laser scan data. Appl. Sci. (Switzerland) 8. https://doi.org/10.3390/app8020263.
Patton, A.I., Rathburn, S.L., Capps, D.M., 2019. Landslide response to climate change in permafrost regions. Geomorphology. https://doi.org/10.1016/j.geomorph.2019.04.029.
Pepin, N., Bradley, R.S., Diaz, H.F., Baraer, M., Caceres, E.B., Forsythe, N., Fowler, H., Greenwood, G., Hashmi, M.Z., Liu, X.D., Miller, J.R., Ning, L., Ohmura, A., Palazzi, E., Rangwala, I., Schöner, W., Severskiy, I., Shahgedanova, M., Wang, M.B., Williamson, S.N., Yang, D.Q., 2015. Elevation-dependent warming in mountain regions of the world. Nat. Clim. Chang. https://doi.org/10.1038/nclimate2563.
Peruccacci, S., Brunetti, M.T., Gariano, S.L., Melillo, M., Rossi, M., Guzzetti, F., 2017. Rainfall thresholds for possible landslide occurrence in Italy. Geomorphology 290. https://doi.org/10.1016/j.geomorph.2017.03.031.
Prokop, A., 2008. Assessing the applicability of terrestrial laser scanning for spatial snow depth measurements. Cold Reg. Sci. Technol. 54. https://doi.org/10.1016/j.coldregions.2008.07.002.
Prokop, A., Panholzer, H., 2009. Assessing the capability of terrestrial laser scanning for monitoring slow moving landslides. Natu. Hazards Earth Syst. Sci. 9. https://doi.org/10.5194/nhess-9-1921-2009.
Rapp, A., 1960. Talus Slopes and Mountain Walls at Tempelfjorden, Spitsbergen: A Geomorphological Study of the Denudation of Slopes in an Arctic Locality.
Rapp, A., Nyberg, R., 1981. Alpine debris flows in northern Scandinavia - morphology and dating by lichenometry. Geografiska Annaler, Series A 63. https://doi.org/10.2307/520831.
Rieg, L., Wichmann, V., Rutzinger, M., Sailer, R., Geist, T., Stötter, J., 2014. Data infrastructure for multitemporal airborne LiDAR point cloud analysis - examples from physical geography in high mountain environments. Comput. Environ. Urban. Syst. 45. https://doi.org/10.1016/j.compenvurbsys.2013.11.004.
RIEGL, 2010a. Data Sheet: Riegl LPM-321 Long Range Laser Profile Measurement System.
RIEGL, 2010b. Data Sheet: Riegl LMS-420i Long Range & High Accuracy 3D Terrestrial Laser Scanner.
RIEGL, 2013. Operating and Processing Software RiScan pro for RIEGL 3D Laser Scanners. RIEGL LMS GmbH.
RIEGL, 2016. Data Sheet: Riegl VZ-6000 – 3D Ultra Long Range Terrestrial Laserscanner with Online Waveform Processing.
Saalmann, K., Thiedig, F., 2001. Tertiary West Spitsbergen fold and thrust belt on brøggerhalvøya, Svalbard: structural evolution and kinematics. Tectonics 20. https://doi.org/10.1029/2001TC900016.
Saalmann, K., Thiedig, F., 2002. Thrust tectonics on Brøggerhalvøya and their relationship to the Tertiary West Spitsbergen fold-and-thrust belt. Geol. Mag. 139, 47–72. https://doi.org/10.1017/S0016756801006069.
Scambos, T.A., Dutkiewicz, M.J., Wilson, J.C., Bindschadler, R.A., 1992. Application of image cross-correlation to the measurement of glacier velocity using satellite image data. Remote Sens. Environ. 42. https://doi.org/10.1016/0034-4257(92)90101-O.
Seneviratne, S.I., Nicholls, N., Easterling, D., Goodess, C.M., Kanae, S., Kossin, J., Luo, Y., Marengo, J., Mc Innes, K., Rahimi, M., Reichstein, M., Sorteberg, A., Vera, C., Zhang, X., Rusticucci, M., Semenov, V., Alexander, L.V., Allen, S., Benito, G., Cavazos, T., Clague, J., Conway, D., Della-Marta, P.M., Gerber, M., Gong, S., Goswami, B.N., Hemer, M., Huggel, C., Van den Hurk, B., Kharin, V.V., Kitoh, A., Klein Tank, A.M.G., Li, G., Mason, S., Mc Guire, W., Van Oldenborgh, G.J., Orlowsky, B., Smith, S., Thiaw, W., Velegrakis, A., Yiou, P., Zhang, T., Zhou, T., Zwiers, F.W., 2012. Changes in climate extremes and their impacts on the natural physical environment. In: Managing the Risks of Extreme Events and Disasters to Advance Climate Change Adaptation: Special Report of the Intergovernmental Panel on Climate Change. https://doi.org/10.1017/CBO9781139177245.006.
Snyder, J.A., Werner, A., Miller, G.H., 2000. Holocene cirque glacier activity in western Spitsbergen, Svalbard: sediment records from proglacial Linnevatnet. Holocene 10. https://doi.org/10.1191/095968300667351697.
Soldati, M., Corsini, A., Pasuto, A., 2004. Landslides and climate change in the Italian Dolomites since the Late glacial. Catena (Amst) 55. https://doi.org/10.1016/S0341-8162(03)00113-9.
Stefan, J., 1890. Probleme der Theorie der Warmeleitung. Sitzungsberichte der mathematisch-naturwissenschaftlichen Classe der Kaiserlichen Akademie der Wissenschaften.
Strand, S.M., Christiansen, H.H., Johansson, M., Åkerman, J., Humlum, O., 2021. Active layer thickening and controls on interannual variability in the Nordic Arctic compared to the circum-Arctic. Permafr. Periglac. Process 32. https://doi.org/10.1002/ppp.2088.
Strömquist, L., 1976. Massrörelser initierade av extremnederbörd ett exempel från andøya i nordnorge. Nor. Geogr. Tidsskr. 30. https://doi.org/10.1080/00291957608551991.
Svendsen, J.I., Mangerud, J., 1997. Holocene glacial and climatic variations on Spitsbergen, Svalbard. Holocene 7. https://doi.org/10.1177/095968369700700105.
Tarini, M., Cignoni, P., Montani, C., 2006. Ambient occlusion and edge cueing to enhance real time molecular visualization. IEEE Trans. Vis. Comput. Graph. 12. https://doi.org/10.1109/TVCG.2006.115.
Telling, J., Lyda, A., Hartzell, P., Glennie, C., 2017. Review of Earth science research using terrestrial laser scanning. Earth Sci Rev. https://doi.org/10.1016/j.earscirev.2017.04.007.
Terzaghi, K., 1950. Mechanism of Landslides.
Tolgensbakk, J., Sollid, J.L., 1980. Kvadehuksletta, geomorfologi og kvartærgeologi 1: 10,000. (Kvadehuksletta, geomorphology and Quaternary geology 1:10,000.). Dept. of Physical Geography. University of Oslo.
Tomczyk, A.M., 2021. Morphometry and morphology of fan-shaped landforms in the high-Arctic settings of central Spitsbergen, Svalbard. Geomorphology 392. https://doi.org/10.1016/j.geomorph.2021.107899.
Turner, J., Marshall, G.J., 2011. Climate change in the polar regions. In: Climate Change in the Polar Regions. https://doi.org/10.1017/CBO9780511975431.
Wheaton, J.M., Brasington, J., Darby, S.E., Sear, D.A., 2010. Accounting for uncertainty in DEMs from repeat topographic surveys: improved sediment budgets. Earth Surf. Process. Landf. 35. https://doi.org/10.1002/esp.1886.
Wichmann, V., 2015. Laserdata LIS Command Reference, Version 3.0.

Wood, J.L., Harrison, S., Reinhardt, L., Taylor, F.E., 2020. Landslide databases for climate change detection and attribution. Geomorphology 355. https://doi.org/10.1016/j.geomorph.2020.107061.

Zangerl, C., Prager, C., Brandner, R., Brückl, E., 2008. Methodischer Leitfaden zur prozessorientierten Bearbeitung von Massenbewegungen. Geo. Alp 5.

Zangerl, C., Eberhardt, E., Perzlmaier, S., 2010. Kinematic behaviour and velocity characteristics of a complex deep-seated crystalline rockslide system in relation to its interaction with a dam reservoir. Eng. Geol. 112. https://doi.org/10.1016/j.enggeo.2010.01.001.